Fall 12-6-2019

LIDAR Assessment to Monitor Bridge Response Under Live and Dead Loads

Daniel Watson
University of Nebraska - Lincoln, daniel.watson@huskers.unl.edu

LIDAR ASSESSMENT TO MONITOR BRIDGE RESPONSE UNDER LIVE AND DEAD LOADS

by

Daniel Watson

A THESIS

Presented to the Faculty of

The Graduate College at the University of Nebraska

In Partial Fulfillment of Requirements

For the Degree of Master of Science

Major: Civil Engineering

Under the Supervision of Professor Richard L. Wood

Lincoln, Nebraska

December 6, 2019

LIDAR ASSESSMENT TO MONITOR BRIDGE RESPONSE UNDER LIVE AND DEAD LOADS

Daniel Watson, M.S.

University of Nebraska, 2019

Advisor: Richard L. Wood

Understanding how a bridge structure responds to various loads in a time and resource-efficient approach is vital in characterizing bridge health. Bridge health monitoring is an evaluation of the structural condition and performance, which optimizes limited transportation budgets by prioritizing the bridges that are in the most need for retrofit or replacement. Identifying and remedying issues will mitigate long-term problems and ensure that the bridge remains open to service for all legal loads. In contrast, health monitoring and load rating will determine if a bridge can only carry traffic up to a certain weight or speed, requiring a bridge load restriction. Bridge response monitored in the field can calibrate a finite element method model to produce more reliable load ratings and distribution factors for bridges. Conventional methods utilizing discrete sensors can be time-consuming and provide a limited view of the bridge response that varies throughout the structure. Full-field data provided by lidar proves to be a viable tool to display the entire bridge response using less time and resources than conventional methods. This thesis evaluates the use of lidar to characterize bridge deflection response under changing live and dead loads. Two bridge structures were monitored while a loaded triaxial truck was placed on the deck and the other two were monitored during a phased construction concrete deck pour. The four assessed bridges represent a wide variety of bridges, where in each

case lidar was able to provide high-fidelity and full-field deflection shapes. For one of these bridge structures, an inverted tee girder bridge of 19.81-meter length, a numerical model was constructed using the known parameters. Using traditional finite element modeling techniques, the numerical model fell short of the physical bridge response under live loads. The numerical model demonstrated the lack of uniform displacement, which was highlighted and characterized in the lidar point clouds. The use of lidar for this bridge structure demonstrates the benefit of the full-field response as well as the simplicity in the load test procedure.

AUTHOR'S ACKNOWLEDGEMENTS

I am extremely appreciative and thankful to the following people who made the completion of my master's thesis possible:

Richard L. Wood, Ph.D., my thesis committee chair and advisor, for allowing me the opportunity to pursue this research and for providing knowledge, advice, and guidance throughout all aspects of this thesis.

Christine E. Wittich, Ph.D., my thesis committee member, for aiding in the collection of the phased construction data, teaching me about lidar collection and processing in your CIVE 898 infrastructure assessment techniques course, and giving your time to review my work.

Cody Stolle, Ph.D., my thesis committee member, for generously giving your time to review my work.

M. Ebrahim Mohammadi, Ph.D. and **Ms. Yijun Liao**, my colleagues, who helped to advise me on collecting and processing lidar data.

George Morcous, Ph.D., P.E., for assisting with data collection in the field, particularly for the *Performance Evaluation of Inverted Tee (IT) Bridge System*.

Nebraska Department of Transportation and **Members of the Technical Advisory Committee**, for guiding Project SG-04 on the *Performance Evaluation of Inverted Tee (IT) Bridge System,* which helped support me as a graduate student to conduct this master's thesis and achieve a master's degree.

The University of Nebraska-Lincoln College of Engineering and **Department of Civil & Environmental Engineering**, for allowing me to pursue my master's thesis and master's degree via the assistantships, fellowships, and scholarships offered.

TABLE OF CONTENTS

LIST OF FIGURES

LIST OF TABLES

NOMENCLATURE

3D	Three-dimensional
AASHTO	American Association of State Highway and Transportation Officials
ACI	American Concrete Institute
C2C	Cloud-to-cloud
cm	Centimeter
DL	Dead load
f'_c	28-day compressive strength
f'_{cr}	Average compressive strength of the mix design
FEM	Finite element method
ICP	Iterative closest point
IT	Inverted tee
kN	Kilonewton
lidar	Light detection and ranging
LL	Live load
LRFD	Load and Resistance Factor Design
LVDT	Linear variable differential transformer
M3C2	Multiscale model to model cloud comparison
MAC	Modal assurance criterion
mm	Millimeter
MPa	Megapascal
SOR	Statistical outlier removal

SfM	Structure-from-Motion
TLS	Terrestrial laser scanner

CHAPTER 1 – INTRODUCTION

1.1 PROJECT OVERVIEW

The purpose of this research project is to assess the use of light detection and ranging (lidar) to monitor, identify, and understand the responses of bridges under changing loads. Guided by methods learned by a literature review, four bridges were monitored under various loading schemes. Two bridge structures were monitored while a loaded triaxial truck was placed on the bridge deck and the other two bridges were monitored during a phased construction concrete deck pour. The two bridges selected for the triaxial truck live loads (LLs) were a single span prestressed inverted tee (IT) girder bridge and a three-span hybrid plate girder and truss bridge. The two bridges selected for the concrete deck pour were a three-span steel girder bridge and a two-span prestressed IT girder bridge. The concrete deck pour is considered a dead load (DL). Monitored bridges were selected to represent a variety of bridge types. The bridge types selected also contained properties and geometries that were predicted to create unexpected bridge responses. Specifically, lidar will provide high-fidelity and full-field deflection shapes that are able to characterize the unanticipated torsional response of bridges where conventional methods cannot. The bridge response for the LL IT girder bridge will be compared to the response from a finite element method (FEM) model created from the design plans using CSiBridge. The results from the numerical assessment will help demonstrate how an uncalibrated FEM model may lead to oversimplification of bridge responses.

1.2 MOTIVATIONS & OBJECTIVES OF RESEARCH

Bridge failure can be catastrophic events leading to injuries and loss of life, such as the collapse of the I-35W Mississippi River bridge in Minneapolis (2007) and the Florida International University pedestrian bridge (2018). These tragic events demonstrate how important structural health monitoring and understanding bridge response can be. Monitoring helps transportation agencies optimize asset inventories which includes bridge structures that may require retrofit or replacement. Monitoring attempts to identify structural health concerns early and fix them to keep bridges open and in service to all legal loads. However, even with consistent and optimal maintenance, a bridge may still demonstrate signs of deterioration as it moves past its design lifespan. When the structural performance of a bridge deteriorates, a bridge may need to be load rated so it can only carry traffic up to a certain weight or speed. In 2016, 10.1% of U.S. bridges required posting of a load restriction (ASCE, 2017). FEM models are one way to produce load ratings and distribution factors for bridges. These models can be improved, in terms of reduced uncertainty, by incorporating measured behavior to produce better results (Shahrooz et al., 1994). Conventional methods used to calibrate FEM models utilize discrete sensors, which can be time-consuming and provide a narrow view of the bridge response throughout the structure. However, lidar can quickly provide a full-field view of the structure, that is not limited to discrete measurement locations. Additionally, the analysis of temporal point clouds collected by lidar can be done to quantify the variation of an area over time (Vosselman & Maas, 2010). This analysis is known as change detection. Change detection can be used to understand the response of a bridge to various loads. To this end, this thesis

will use lidar to characterize the response of bridges under changing live and dead loads and compare one of the bridges to a FEM model prediction of the response.

1.3 PROJECT OUTLINE & SCOPE

This thesis consists of six chapters. Chapter 2 describes a literature review on lidar, point clouds, and change detection; finite element method; and an example case study on phased construction. The literature review sets up the framework for this project. Chapter 3 introduces live load testing using discrete sensors and compares it to full-field monitoring. Chapter 4 compiles the general information and instrument setup, a summary of results and discussion, and key findings for each of the four bridges monitored using lidar. This chapter gives overall conclusions for the use of lidar assessment to monitor bridge response encapsulating changing live and dead loads. Chapter 5 encapsulates the FEM model description, summary of results and discussion, and conclusions for the 19.81-meter IT girder bridge numerical assessment. The model will be evaluated by comparing it to the lidar results from the previous chapter. Chapter 6 presents the final project conclusions as well as offers recommendations on future work topics related to this research.

CHAPTER 2 – LITERATURE REVIEW

2.1 LIDAR, POINT CLOUDS, AND CHANGE DETECTION

Light detection and ranging (lidar) is a remote-sensing technique used in multiple fields (e.g., engineering, construction, archaeology, earth and planetary sciences, etc.). Lidar has a wide range of uses due to its ability to quickly and accurately create large point clouds or sets of three-dimensional (3D) vertices in space. The lidar data, also known as laser scanning data, can be broadly categorized into three types based on collection platform: static or terrestrial laser scanning, kinematic or mobile laser scanning such as mounted on a vehicle, and airborne scanning on a manned or unmanned aerial system (Vosselman & Maas, 2010). The terrestrial platform is the best platform to measure bridge response due to the relatively small amount of area being scanned, and the required accuracy at the millimeter (mm) level (Liao et al., 2019). Terrestrial laser scanners (TLSs) can be broken into three categories based on how the scanner computes distance (Vosselman & Maas, 2010). Triangulation-based measurement calculates distances on the target using a camera and laser spaced at a known distance apart and with known angles to the target. Time-of-flight emits a powerful pulse of laser light and identifies the time between emission and detection to measure distance by using the speed of light. Phase-based emits a continuous wave that has its frequency or amplitude modulated. When the wave reflects off a surface and returns, the distance is calculated by demodulating the wave to measure the phase shift.

When performing a lidar scan, there are four major groups of influencing factors: 1) scanner mechanism which is influenced by hardware properties, calibration, and settings; 2) atmospheric conditions and environment that are influenced by humidity,

temperature, and pressure; 3) object properties such as reflectivity and roughness of the target surface; and 4) scanning geometry which is impacted by location and orientation of the surface compared to the scanner (Soudarissanane, 2016). The instrument specifications will list the scanner mechanism and the acceptable range of atmospheric conditions in which those specifications will be met. Object properties cannot be controlled when capturing an object because the reflectivity and surface roughness are constant. However, it is important to note surfaces which may not be captured as well, because these areas will require additional processing and filtering.

The lidar data collection strategy can be partially controlled by attempting to place the scanner at the lowest incident angle to the area of interest. As the incident angle increases, the point density will be lower, and the points may poorly represent the structure due to beam scatter. The theoretical number of points begins to decrease dramatically for orientations greater than 70º, which impacts the standard deviation of the points, as shown in Figure 2.1 (Soudarissanane, 2016). Note that the point density is also a function of the distance from the scanner. The closer the scanner is to the area of interest, the higher density and typically more accurate the point cloud will be. Although standard deviation is not precisely synonymous with accuracy because it is possible for a group of points to have a low standard deviation but poorly represent the actual structure. Lõhmus et al. compared TLS with that of precise leveling for two bridges and concluded that TLS point clouds could be carried out with an accuracy of 1 mm. However, it was also identified that some monitored points had much larger (up to 3.4 mm) discrepancies for one of the bridges. Their study concluded that this inaccuracy was caused by a larger incidence angle, eccentric placement of the leveling marks on the bridge deck, different deformation

behavior of the bridge deck than the bridge beams (the precise leveling was performed on the deck while the lidar was performed on the girders), and asymmetric placement of the load with respect to the bridge deck and the two beams (Lõhmus, Ellmann, Märdla, & Idnurm, 2018). While this work provides some certainty on the application of lidar for bridges at the mm level, this differs from the work in this thesis due to scope. Herein, the focus is on applying lidar with change detection to draw conclusions on the response of bridges under various load scenarios. However, it is important to note that if the accuracy of the point clouds and the processes the point clouds undergo are not precise enough, conclusions cannot be reliably drawn. For example, if the lidar accuracy is only on the cm scale, but the deflection of the bridge is on the mm scale, conclusions on the bridge response are not reliable, and a more robust method for monitoring the bridge should be conducted.

After the lidar scans are performed, they can be uploaded as a point cloud to a visualization and processing software (e.g., CloudCompare, Meshlab, FARO Scene, Leica Cyclone, etc.). Some of the software platforms require paid licenses, while others are opensource. Within a selected software platform, the point clouds should first be filtered and then registered using appropriate methods. Filtering can be executed with regards to geometry, distance, intensity, nearest neighbor, etc. Geometry-based filtering splits the point cloud based on the location of the points in 3D space, typically via a manual noise removal. This is usually performed to remove points not in the area of interest or in areas that the user knows are noisy due to the laser scanning influence factors mentioned previously. Distance-based consists of removing points based on Euclidean distance from a reference point, typically the scanner. This removes the noise caused by an increase in

uncertainty when a point is located farther from the scanner. Intensity-based removes points based on the value of the reflection intensity. This removes statistically inaccurate points that can be caused by weak reflections due to distance, angle of incident, material surface, etc. Nearest-neighbor filtering attempts to remove stray points that are relatively far from other points in the point cloud. One type of nearest-neighbor filter is a statistical outlier removal (SOR), which fits a plane to a specified number of its closest points in the cloud and then removes the point if it is too far away from the fitted plane (Girardeau-Montaut, D., 2015). The SOR tool in CloudCompare is similar to the sparse outlier removal used by Rusu et al. to improve their point cloud registration results by removing only the most erroneous 0.36% of points (Rusu, Marton, Blodow, Dolha, & Beetz, 2008). Rusu et al. state that sparse outliers complicate the estimation of local point cloud characteristics leading to erroneous values, which may cause point cloud registration failure.

Once appropriate filtering has been done to remove unwanted or noisy points, scans can be registered by point-based or target-based, fine registration or ICP, or feature-based techniques (Vosselman & Maas, 2010). Point-based aligns scans by selecting points appearing in both scans that have known correspondence. This is typically performed manually, although some software can identify corresponding points when targets are used. Targets can be placed in the surrounding area to aid in alignment, especially if the environment does not have distinguishing features. Point-based registration uses a relatively small percentage of the points to register the point clouds in comparison to ICP registration, which uses the entire overlapping portion of the clouds. ICP registers a data shape with N_p points to a model shape with N_x primitives. This can be a set of points, polylines, parametric curves, triangles, parametric surfaces, or implicit surfaces (Besl &

McKay, 1992). The ICP algorithm converges to the minimum point-to-point distance for the overlapping points in the different clouds. Feature-based alignment uses geometric primitives such as planes, spheres, or cylinders that are identified in each point cloud. For this, only the points within the geometric primitives are used to align the scans by minimizing their point-to-point distances.

Change detection and deformation monitoring is the process used to compare two or more point clouds to see how they differ temporally. Change detection looks for a binary answer, i.e., did the situation change or not, whereas deformation analysis looks for a quantified change (Vosselman & Maas, 2010). Application wise, lidar with change detection has been used more to characterize and monitor relatively large changes such as on a centimeter (cm) or decimeter level and for hard surfaces since change detection often struggles with non-static objects like moving vegetation due to wind, water, etc. Jaboyedoff et al. highlights how TLS is being used to detect, assess, model, and monitor hard surfaces such as landslides, rockfalls, and debris flow by removing vegetation (Jaboyedoff et al., 2012). However, as lidar technology and change detection methods have improved to be more accurate, it has enabled small-scale, on the mm order, level of change detection which is needed to monitor bridge response and other civil structures.

The CloudCompare tool called cloud-to-cloud (C2C) distance uses octrees and an algorithm similar to Hausdorff distance algorithm to compare the two point clouds and calculate distances (Girardeau-Montaut, D., 2015). Octrees are an efficient data structure for spatially indexing large point clouds to enable improved efficiency for data manipulation needed to perform the Hausdorff distance algorithm (Vosselman & Maas, 2010). Hausdorff distance is slightly slower than other common methods to calculate

distance, such as average distance and best-fitting plane orientation, but its advantage is that it is more precise (Girardeau-Montaut, Daniel, Roux, Marc, & Thibault, 2005). Hausdorff distance computes the distance from each point p of a cloud S to its nearest point p' in the comparison cloud S'. Another method to compare point clouds is by a multiscale model to model cloud comparison (M3C2). M3C2 computes the local distance between two point clouds along the normal surface direction which tracks 3D variations in surface orientation (Lague, Brodu, & Leroux, 2013). Lague et al. state that unlike C2C, the method is robust to changes in point density and point cloud noise. However, the point clouds produced in this work are dense due to using TLS and with a low level of noise due to favorable target object properties. Thus, C2C using Hausdorff distance will be used to find the absolute distance between two measured points instead of an approximation of the distance based on surface normals.

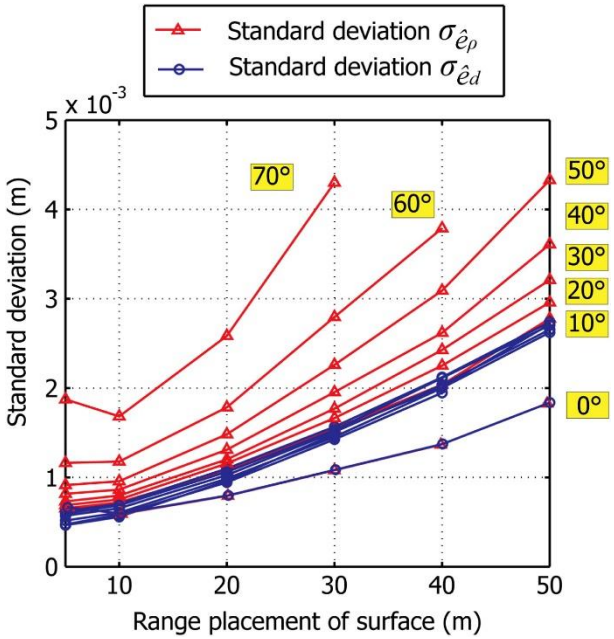

Figure 2.1: Standard deviation with respect to the incidence angle of the surface in the direction of the laser beam (red) and after removal of the incident angle effect (blue) (courtesy of Soudarissanane, 2016).

2.2 FINITE ELEMENT METHOD

Bridges are large, complex structures whose response would be poorly represented if it was lumped as a whole unit. Therefore, the FEM is commonly used as a numerical method to subdivide a large system into smaller, simpler parts. The small parts accumulate into a large system of equations that model the entire structure. FEM is commonly used for multiple bridge applications including determining load distribution factors, load rating, and overall prediction of the bridge response (Sanayei, Phelps, Sipple, Bell, & Brenner, 2011; Zokaie, 2000). Therefore, there is a plethora of free and commercial software that can be used to model a bridge including ADINA, Ansys, FreeCAD FEM, RFEM, SAP 2000, and CSiBridge. Many of the software platforms, including CSiBridge, utilize shell elements to model the bridge deck. Each shell has independent membrane and plate behavior, and the membrane deformation within each layer uses a strain-projection method (CSI, 2016; Hughes, 2012). Hughes created the widely adopted bilinear displacement model to estimate displacement. Bilinear displacement and rotation functions are employed in conjunction with selective reduced integration which allows it to be very simple yet accurate. Girders can be modeled by either shell elements, beam elements, or a combination of the two. For example, a girder can be modeled with the web as a shell element and the flanges as beam elements. Girders can also be modeled as either linear or quadratic elements. Chung et al. modeled eight simply supported I-beams subjected to a concentrated load at the center span, varying the model to have shell or beam elements with linear or quadratic modeling. They found that if the number of degrees of freedom is high enough, all methods will converge on the analytically correct deflection in the linear range. However, Chung et al. found that quadratic elements are typically more accurate

than line-elements for the same mesh density. It was also identified that shell elements will require a higher level of mesh refinement to converge than beam elements (Chung & Sotelino, 2006). The study suggests that any method used to model the girders will be accurate with a sufficiently high mesh density, although a higher mesh density will require a large computational demand. Typically, rigid connections are used to connect different elements of the structure, so they deflect as a unit (e.g., the connection of deck to the girders). Prestressed tendons are typically modeled as tendon objects, which are a special type of object that can be embedded inside other objects (frames, shells, planes, etc.) and impose loads upon those objects (CSI, 2016). The boundary conditions caused by the abutments are often the most difficult thing to predict as the abutments typically behavior somewhere between a fully-fixed and pinned joint. To account for this, the boundary conditions can be modeled as restrained, free, or spring conditions.

In addition to the unknowns and assumptions above, which can cause inaccuracies in a model (e.g., the end restraints), some input parameters that are on the design plans do not represent the existing structure and should be updated to make a more realistic model. For example, initial FEM models will typically use the lower bound for the elastic modulus of concrete and do not account for the contribution of the reinforcement steel, the hardening of concrete over time, and the uncertainty of the initial pour. Usually, the compressive strength of the concrete is taken as the 28-day compressive strength, f'_c. However, this is a conservative estimate, as Figure 2.2 shows concrete continues to gain some strength over time. In this figure, f'_c is boxed, and the gain in compressive strength is displayed as a percent increase (from the 28-day strength) for the concrete samples older than 28-days. The strength gain occurs when moisture is provided by rainfall and other environmental

sources such as high humidity. This conservative estimate of strength is compounded by the ACI (American Concrete Institute) 318 strength requirement, which states that the average compressive strength of the mix design, f'_{cr}, must have a reasonably high probability to exceed the specified value of f'_c. The amount that f'_{cr} must exceed f'_c varies based on the standard deviation of tests and strength of concrete required (an f'_c greater than 35 megapascals (MPa) uses a different set of equations than an f'_c less than 35 MPa). Figure 2.3 displays a few examples of how f'_c and f'_{cr} are related through the coefficients of variation. Note that there is a very high chance the concrete poured on a bridge is marginally higher, and there is a very low chance the strength is equal or less than the design strength.

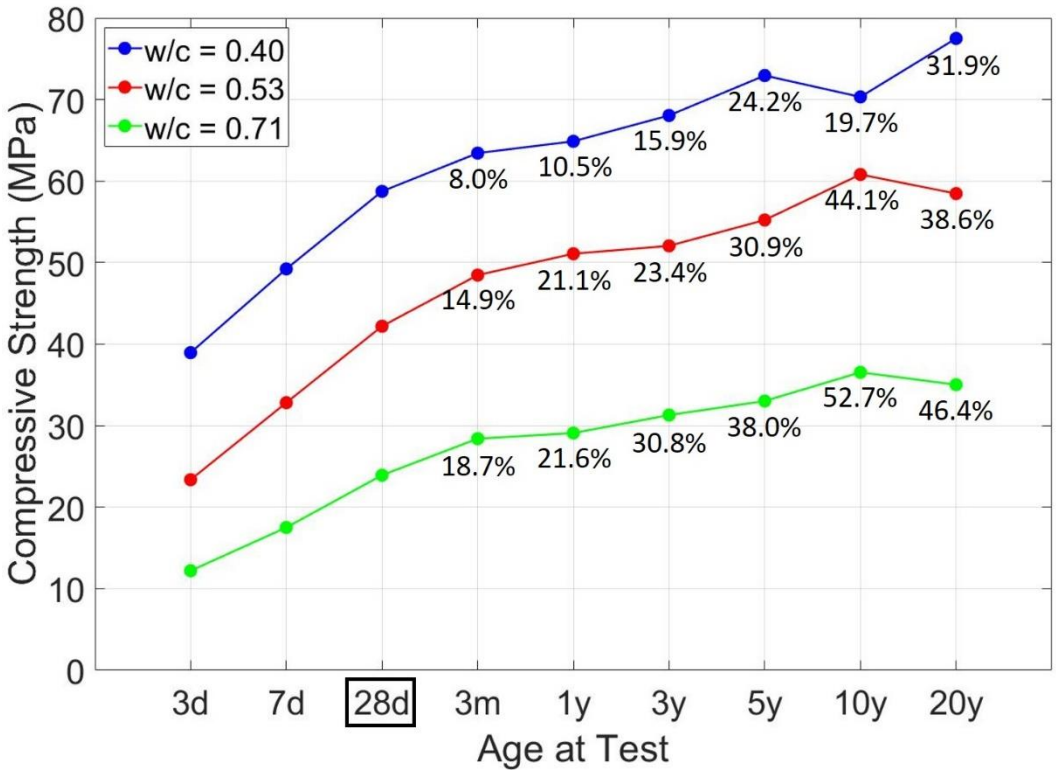

Figure 2.2: Concrete compressive strength increases as it ages in outdoor exposure in Skokie, Illinois for Type I cement (recreated from Wood, 1992).

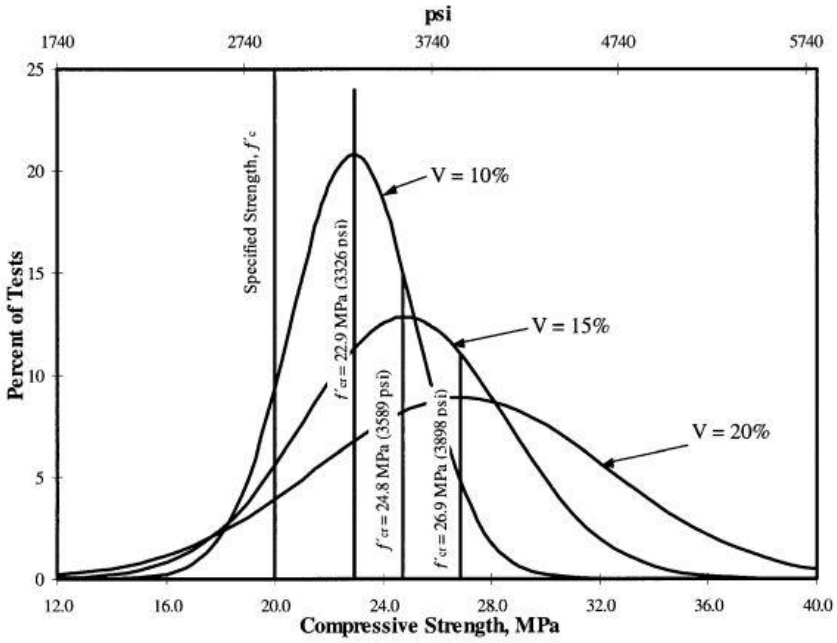

Figure 2.3: Minimum required average strength for a specified design strength (courtesy of ACI (American Concrete Institute), 2011).

2.3 PHASED CONSTRUCTION CASE STUDY

Phased construction is used for bridge construction to minimize the impact on traffic flow because part of the bridge is replaced while the other half is being used for through traffic. This section will be a case study on problems associated with phased construction and the reason that they occur. Problems resulting from phased construction methods can be broken up into two sections: short-term constructability concerns and long-term structural performance. Short-term constructability concerns can occur as a differential elevation at the time of closure and/or torsional distortion of individual phases. Differential elevation at the time of closure means that the phases meet at the phasing line at a different elevation, while torsional distortion occurs when one or both phases rotate, usually rotating away from the other phase. These concerns are important because significant differentials and torsional distortion can cause difficulty in pouring the closure

region, splicing of the transverse reinforcement, installing cross-frames, and may potentially reduce the durability of the phase-line joint. Difficulty in pouring the closure region can cause an incorrect transverse deck profile and cross slope, reducing the drainage potential of the deck. In addition, if torsional distortion is large enough, there is a potential to cause gross instability in the bridge by creating an unsymmetrical cross-section that if large enough, could cause structural deterioration.

Differential elevation can come from multiple sources. Some of these sources are easy to quantify and compensate for, while others can be more difficult. The easiest source to identify and correct is construction errors or tolerances (e.g., girder seat elevations, camber, etc.), design oversight, and construction sequencing. More difficult sources to identify or predict come from those associated with time-dependent deflections occurring between the construction of the two phases. This includes creep, shrinkage, settlement, loss of restraint behind the turndown, and temperature and seasonal effects. These sources can be difficult to estimate and quantify since it requires continuous monitoring and record-keeping, which is often not done due to limited resources. An example of how creep and shrinkage cause differential deflection is shown in Figure 2.4. Phase I is very close to its permanent self-weight deflection, whereas phase II has not yet reached its permanent deflection leading to the difference in elevation. Also note that the closure pour is poured before phase II has undergone all the creep and shrinkage effects, which can cause additional stresses in the closure region and cross-frames post-construction. Torsional distortions can be caused by the unsymmetrical placement of the deck over the girder pattern for an individual phase or by the placement of unsymmetrical loading with the

addition of temporary and placement barriers. Unsymmetrical geometry or loading causes the bridge to rotate.

Azizinamini et al. studied the deflection of a Dodge Street Bridge over I-480 in Omaha, Nebraska, where eight continuous steel plate girders spaced at 2.87 meters span two equal spans of 72.09 meters. The bridge deck was being replaced via phased construction. They predicted the deflection of the bridge using a FEM model which attempted to account for shrinkage, creep, and aging. The shrinkage data was input as the average unrestrained shrinkage strains obtained from control specimens from concrete used in the positive region pour. The creep coefficients were estimated using the ACI empirical model equation 6-5, assuming the concrete age at loading was 20 days and with no adjustments for humidity, slump, or other factors. An aging coefficient of 0.8 was used throughout. The deflection caused by each of the individual inputs were summed together, and the predicted deflection is shown in Figure 2.5. In this figure, the predicted deflection was compared to the experimental bridge deflection, which was monitored using potentiometers. Differences were noted up to 45% at 90 days. Note that the removal of forms was not considered in the predicted deflection profile, which would have caused the results to be closer together. However, before the removal of the forms, the prediction overestimated deflection by 20% at 25 days. These figures show that even with a detailed effort to predict the amount of deflection caused by shrinkage, creep, and aging, it is difficult to predict the total amount of deflection due to uncertainty of the input parameters. The difficulty in prediction makes the elimination of differential elevation and torsional rotation in phased construction nearly impossible. However, careful monitoring of bridge

behavior may aid in mitigating the issue by allowing for corrective action in the beginning stages before it becomes too severe.

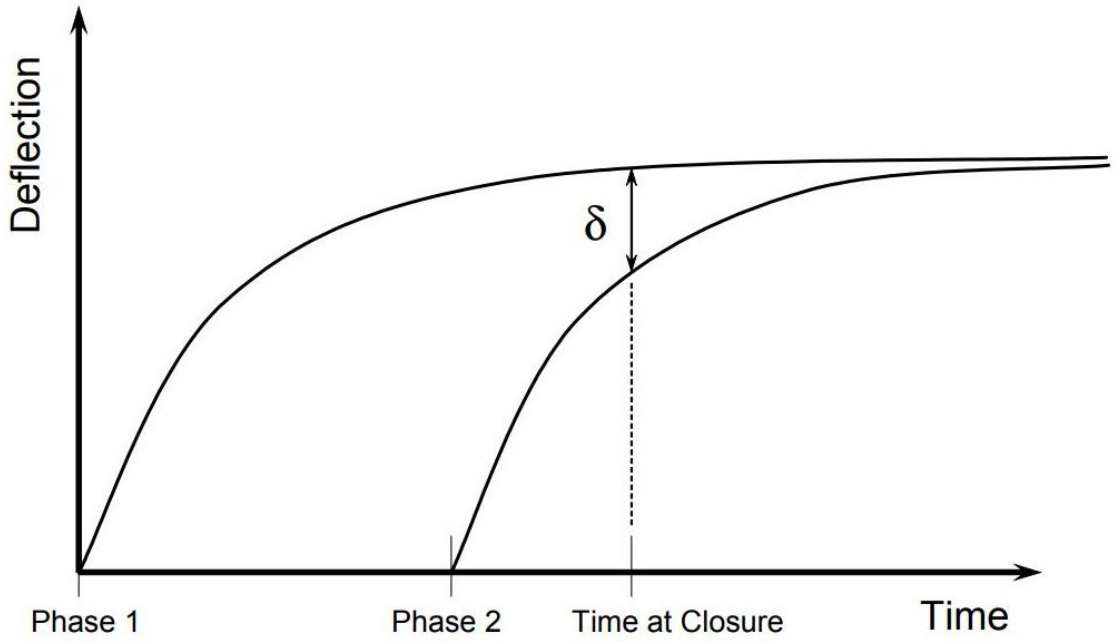

Figure 2.4: The differential deflection caused by creep and shrinkage (courtesy of Azizinamini, 2003).

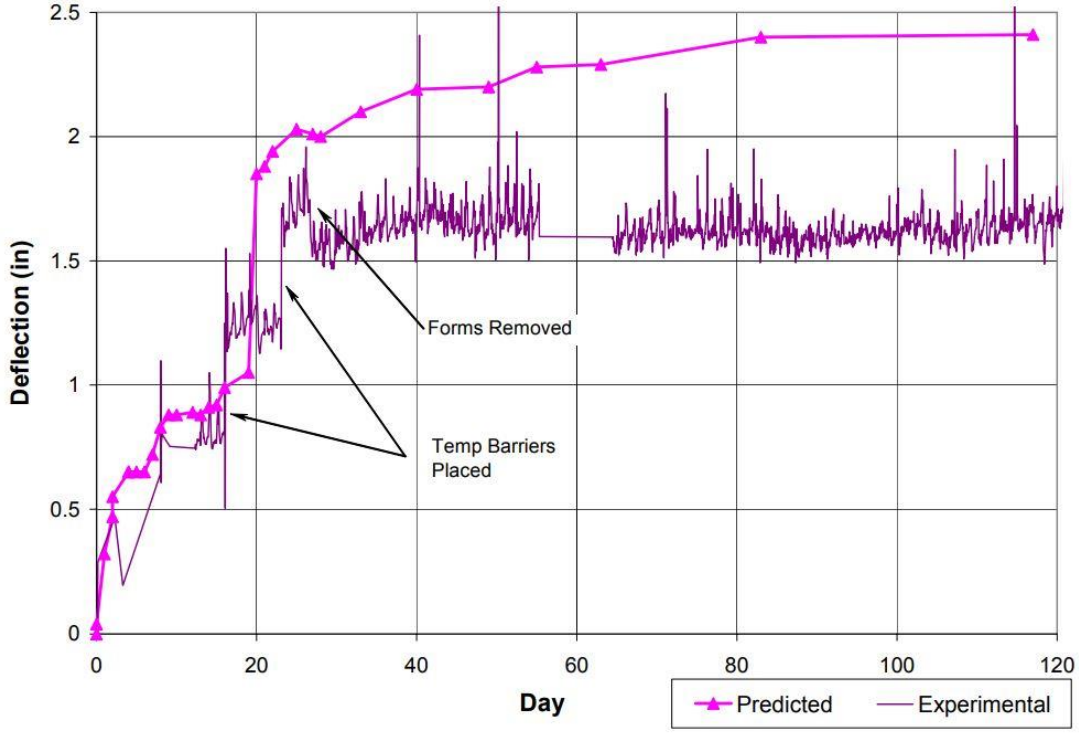

Figure 2.5: Comparing the predicted deflection with the actual deflection over time (courtesy of Azizinamini, 2003) (1 inch = 2.54 centimeters).

2.4 APPLICATION TO THE THESIS

This literature review chapter laid the groundwork to complete this work contained within this thesis. The lidar point clouds and change detection sections aided in the collection and processing of the lidar data. The scanners used to collect the data were the Faro Focus^{3D} x130 and s350 lidar scanners, based on equipment availability within the research group. These phased based scanners have the specifications listed in Table 2.1. The literature review guided the scanner placement in the effort to get the scanner as close to the center of the span of interest while also trying to limit the angle of incident to create a denser cloud in the area of interest. However, as shown in Figure 2.6, placement at the center of the span of interest was not possible for all bridge locations as it is not ideal to place the lidar scanner in water. Therefore, the scanner was placed on the bank at a safe distance away from the water. The atmospheric conditions and environment were also controlled during the scanning by taking the scans within the range of acceptable temperatures and in non-condensing humidity environments. This section aided in filtering using primarily a geometry-based technique, registration using point picking via manual selection on the abutments or piers with the assumption that these locations undergo negligible deflection under the loading, and change detection using C2C. The operations were performed using both CloudCompare and FARO Scene. This process resulted in the figures shown in Chapters 4 and 5.

The FEM literature review guided the creation of the model in Chapter 5 by aiding in the selection of appropriate model parameters. CSiBridge was selected due to its ease of use and specialization in creating bridge models. The phased construction case study developed a background on what to expect from the phased construction change detection

results in Chapter 4. The case study also highlighted the problems associated with the differential deflection and torsional rotation caused by creep, shrinkage, and aging which are difficult to control due to the high degree of uncertainty. Lidar with change detection may prove to help monitor and document the response of bridges caused by the phased deck pour and assist in problem mitigation.

Table 2.1: Performance specifications for the Faro Focus^{3D} x130 and s350 laser scanners (Faro, 2011).

Specification	**x130**	**s350**
Range	0.6 to 130 m	0.6 to 350 m
Maximum Recording Rate	976,000 pts/sec	976,000 pts/sec
Ranging Error (Points @ 10 to 25 m)	± 2 mm	+/- 1 mm
Camera Resolution	170-megapixel color	165-megapixel color
Vertical Field of View	300º	300º
Horizontal Field of View	360º	360º
Minimum Angular Resolution	0.009º	0.009º
Laser Class	1	1
Wavelength	1550 nm	1550 nm
Beam Divergence	0.011º	0.017º
Beam Diameter at Exit	2.25 mm	2.12 mm
Ambient Temperature	5º to 40º C	5º to 40º C
Humidity	Non-condensing	Non-condensing

Figure 2.6: Faro Focus^{3D} s350 laser scanner setup.

CHAPTER 3 – LIVE LOAD TESTING

3.1 INTRODUCTION

Live load testing can be used for structural assessments such as modifying or confirming load ratings for bridges and evaluating distribution factors. LL testing is commonly used to check and calibrate the FEM models highlighted in Chapter 2.2. It helps reduce the uncertainty within model calibration by providing direct response measurements of the bridge structure under known LL. This helps to provide constraints on bridge parameters including the amount of composite action, fixity at supports and over piers, significance of cracked concrete, etc. For example, distribution factors calculated using the American Association of State Highway and Transportation Officials (AASHTO) Load and Resistance Factor Design (LRFD) Bridge Design Specifications do not include secondary bridge elements such as barriers, curbs, or diaphragms. These secondary bridge elements have been shown to increase the LL distribution, usually causing a decrease in girder strains (Roddenberry, Chipperfield, & Tawfiq, 2011). This chapter will review some of the discrete sensors traditionally used to assess bridges and compare them to full-field monitoring techniques.

3.2 DISCRETE SENSORS

Many types of equipment can and have been used to monitor LL testing. The section will focus on three of the more commonly used discrete sensors for LL testing: linear variable differential transformer (LVDTs) that measure deflection, strain gauges that measure the strain, and accelerometers that measure vibration. Figure 3.1 displays an LVDT, strain gage, and accelerometer setup example on bridge girders.

A disadvantage for all the aforementioned methods is that direct placement of the equipment on the structure is needed. This is especially true for LVDTs, which need to not only be attached to the bridge, but also connected to a stable reference point to measure the deflection. This makes it difficult to measure bridge deck deflection. The placement of strain gauges and accelerometers is fairly easy for measuring the response of the deck but measuring the response of the girders underneath the bridge can be much more difficult. To record maximum bridge responses, sensors need to be placed at the midspan of a simply-supported bridge or at other predetermined locations for non-simply supported bridges. For easy setup, this requires that the bridge has a sufficiently low clearance where the midspan can be reached either by standing or using a ladder permitting a sufficiently low ground grade and low ordinary high water elevation. If the bridge has a high clearance, a platform vehicle will be needed in order to correctly place the equipment, which requires more manpower, effort, and time.

Another disadvantage for all the previously mentioned discrete sensors is that they can only collect data over the very small region where it is placed. The placement of equipment may not be a good representation of the entire bridge response, depending on how the bridge was loaded, how the bridge typically responds, and the number of sensors used. Moreover, this identifies the need to know the exact target location for the measurement – which can vary or be unknown for certain bridges. Specifically, bridges with unique responses will be more difficult and will need many sensors to make sure the bridge response is well represented. For example, to validate their FEM model and show that the AASHTO distribution factors for a bridge were conservative, Hodson et al. used 56 strain gauges on the superstructure of a box-girder bridge (Hodson, Barr, & Pockels,

2012). Using their calibrated FEM model, they concluded that AASHTO LRFD interior girder distribution factors were conservative by 3.6 and 9.4% for positive and negative moments, respectively. Although these results are likely accurate due to the number of sensors used, it is a time-consuming process and unreasonable to expect this level of effort to be taken for all bridges with the limited resources for bridge monitoring. Additionally, even with the placement of numerous sensors, most discrete sensors methods will be unable to catch some of the behaviors such as rotation of individual girders. Monitoring rotations can be important because rotation can cause both local and global instability of the girders and the bridge. For example, exterior girder rotations, particularly during bridge construction, can be caused by the overhang portion of the deck. The overhang portion of the deck produces an unbalanced eccentric load, thereby causing instability in the bridge.

The setup for all LL testing methods is important; however if done incorrectly, it can introduce errors and biases in the collected data. Discrete sensors only measure response in a particular direction. This means that any tilt or offset in placing the equipment can cause errors by lessening the magnitude of the measured deflection, acceleration, or strain. Additionally, strain gauges and accelerometers rely on adhesion to rigidly connect to the structure, while LVDTs rely on a stable, stationary base. If the strain gauges and accelerometers are not rigidly connected, noise will be created as the equipment fluctuates independently of the structure. In addition, the slip of adhesion will cause long-term drift, or long-period oscillations, as the equipment moves away from the structure which will need to be filtered out during the processing stage. Long-term drift can likewise occur for LVDTs due to equipment settling over time if the base is not properly grounded.

a)

b)

Figure 3.1: Accelerometer, LVDT, and strain gauge installation example for a) far and b) near views.

3.3 FULL-FIELD MONITORING

Full-field monitoring techniques such as digital image correlation and lidar create results that represent the entire structure. Full-field monitoring techniques represent the

entire structure by collecting 3D data. An example of the 3D representation from a lidar scanner viewpoint is shown in Figure 3.2. Notice the structure has been created by many points or vertices, each containing a position in 3D space, color, and intensity data. This means that nearly the entire bridge span will have positional data, whereas discrete sensors only collect data at specific locations where the equipment is placed. Having a full-field view is an advantage because the entire bridge response can be observed. This makes it easier to see how the bridge is responding in its entirety and unexpected responses will not be missed.

Unlike discrete sensors, full-field monitoring techniques do not take much preparation or set up to collect data. Quite simply, the camera or scanner just needs to be set on top of a tripod and have the appropriate setting selected to collect data. Shown in Figure 3.3, digital correlation is set up and can take images before and after loading in order to measure the deflection. Similarly, lidar can be set up and take a scan before and after the loading is applied. Full-field monitoring techniques also have fewer limitations in collecting data. Unlike discrete sensors, they do not touch the structure to collect data. Therefore, full-field monitoring techniques can gather data for bridges with high clearances or structures that have the midspan blocked by water for which other methods would require a platform vehicle.

On the other hand, full-field techniques also have some disadvantages. The primary disadvantage of full-field techniques is that they can currently only collect static or quasi-static information due to the time required to collect the data. Static measurements are seldom used alone to quantify bridge response because bridges respond differently to static and dynamic loading. For example, Schlune et al. observed that bearing behavior was

different under ambient excitation and during the load tests. Therefore, it was not possible to update the boundary condition for their FEM model through modal characteristics and then use the same boundary conditions for static analysis. They concluded that the combination of numerous and diverse kinds of measurements should preferably be used when a generally valid FEM model is sought (Schlune, Plos, & Gylltoft, 2009). Additionally, the bridge will have to be shut down to collect data while a static load is placed on the structure. This will require extra coordination with transportation agencies to safely close the bridge whereas some discrete methods will not need to stop traffic. For example, accelerometers do not need to shut down bridges because they utilize the ambient vibration of normal everyday traffic to collect data on bridge behavior (Fu & He, 2001).

The full-field techniques also have an advantage over discrete sensors by making results easy to visualize, even for people not familiar with structural analysis. For lidar, the point clouds for unloaded and loaded cases can be segmented to display only the girders. The segmented girders can be compared using change detection to see how the bridge responds on a point by point basis. Figure 3.4 shows the deflection of a skewed hybrid high-performance bridge caused by two static trucks placed on top of the deck. The figure makes it easy to visualize that the exterior girders, where the truck is located, deflects the most while the other side of the bridge barely deflects. Liu et al. used the lidar measured displacements to validate that the bridge experiences tolerable displacements under specified loads. In addition to the full-field figures, cross-sections can be segmented out of point cloud to display cross-section behavior. The cross-section behavior can be used to more easily visualize responses such as girder rotation, which most discrete sensor methods do not directly measure, or adjacent girder differential deflection.

The full-field monitoring techniques can produce accurate enough results to quantify bridge response. Albert et al. tested the applicability of single image photogrammetric approaches to bridge deformation measurements. They were able to show precision potential in the order of 1:200,000 to 1:300,000 of the monitored field of view could be achieved (Albert, Maas, Schade, & Schwarz, 2002). Similarly, Lõhmus et al. monitored the bridge deformations for two bridge using TLS and compared the results to precise leveling, reflectorless tacheometry, and dial gauges to test its accuracy. They identified that although TLS results should be verified by other methods when a sub-mm accuracy is required, the TLS data provided sufficiency accuracy to be used as an additional survey method for load tests. In addition, they concluded that since the entire area of interest is covered with continuous high-resolution data, it is capable of detecting unexpected deformations in areas where the sparse point-wise techniques may miss them entirely (Lõhmus et al., 2018).

Another form of full-field monitoring is Structure-from-Motion (SfM), which is a photogrammetric range imaging technique that generates a point cloud. SfM creates a point cloud by identifying the same point in two or more images. Using the identified points, the relative location of the cameras can be triangulated. With the known camera locations, the corresponding points that have been identified as the same in two or more images will become points in the 3D point cloud. The process to turn images into point clouds can be performed in open-source software such as Visual SfM or Bundler or commercial software such as Photomodeler or Agisoft Photoscan. SfM obtains the best results when: 1) there is significant overlap between adjacent images (70-90%); 2) each image in a set is verifiable by at least one other image; 3) there are distinct and accurate reference points in the images

to scale the point cloud; 4) a high-quality camera is correctly used; 5) the target surface has distinct features with edges and varying textures; and 6) capturing images with appropriate lighting (Raugust & Olsen, 2013).

SfM has several hindrances in comparison to lidar. First, scaling is subject to human error because the point cloud is originally unitless, whereas lidar built into data collection. Second, SfM is typically less accurate than TLS. James et al. showed that SfM with multiview-stereo algorithms could have a relative precision of roughly 1:1000 or better. This ratio yields a cm-scale precision for viewing distances on the 10's of meters scale. They conceded this is not as precise as TLS techniques but can be used as a low-cost viable alternative when the highest degree of precision is not required (James & Robson, 2012).

Additionally, if the processing software can not fit the images together due to the inability to find common features, multiple models may be created on different reference frames. Since the processing software can take significant time to process the images into a point cloud, the failure in image collection will not be known on-site, and an additional trip to the site will need to be taken to collect the necessary images. This differs from lidar because lidar scanners have a preview feature allowing the point cloud to be viewed on-site, and a scan can be retaken if part of the structure is missing from view.

In conclusion, full-field monitoring techniques are able to quantify bridge response in a quicker and easier setup and create 3D representations of structures that lead to easy to visualize results in comparison to discrete sensors. Out of the full-field monitoring techniques, lidar is the most suitable for monitoring the response of bridges under loading due to the higher data collection accuracy compared to photogrammetric techniques.

Additionally, lidar eliminates some sources of error that exist in photogrammetric techniques, such as scaling and point cloud processing failures.

Figure 3.2: Example of 3D representation.

Figure 3.3: Machine vision CCD camera setup (courtesy of Albert et al., 2002).

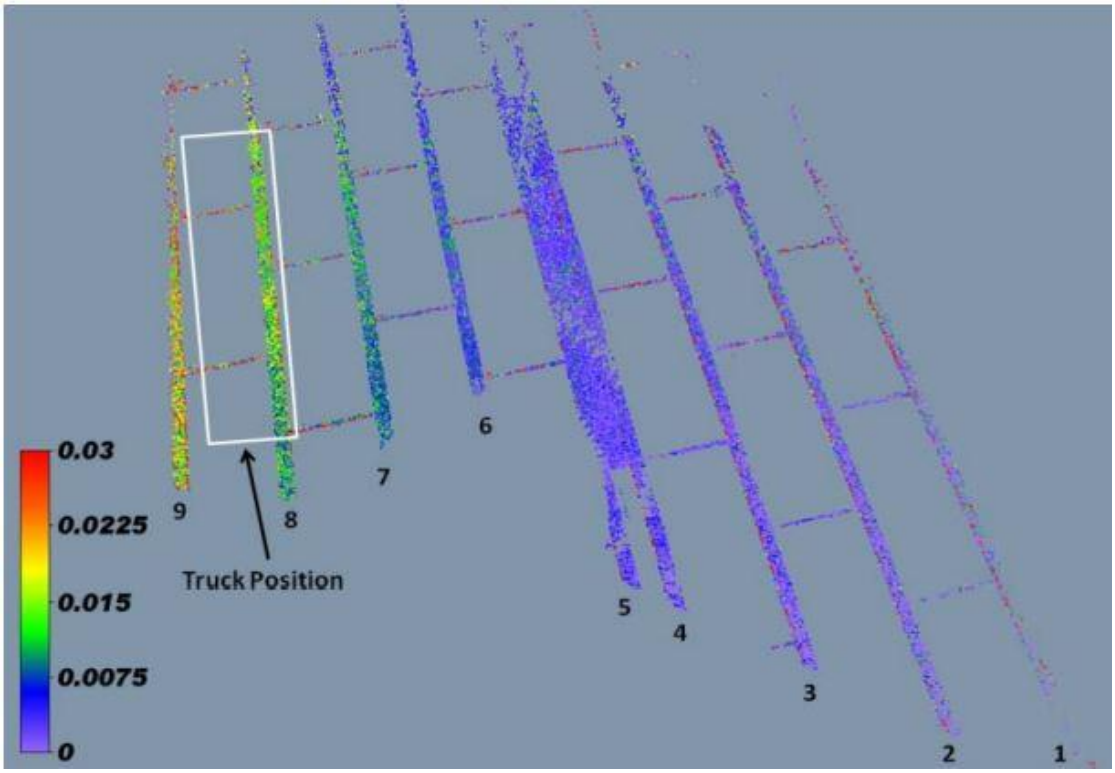

Figure 3.4: Example of easy visualization (courtesy of Liu, 2010).

CHAPTER 4 –BRIDGE MONITORING USING LIDAR

4.1 INTRODUCTION

This section will use lidar to quantify the bridge responses of the four bridges shown in Table 4.1. The first and last bridge structures monitored were responding to a loaded triaxial truck being placed on the deck, while the middle two bridges were monitored during a phased construction deck pour. These bridges were selected to represent a well-diversified group and were loaded to create unanticipated bridge responses. To obtain the best results, the creating, filtering, and aligning point clouds will use the process outlined in the literature review in Chapter 2.1.

Table 4.1: Monitored bridges summary.

Bridge Name	Bridge ID	Bridge Type	Load Type
Little Blue River	S005 00446	68.28-Meter 3-Span Hybrid Plate Girder and Truss Bridge	Live Load
Brunswick	S014 17044	34.44-Meter 3-Span Steel Girder Bridge	Deck Pour
Silver Creek	S030 35969	36.58-Meter 2-Span Prestressed IT Girder Bridge	Deck Pour
Elk Creek	C002408505	13.91-Meter Single Span Prestressed IT Girder Bridge	Live Load

4.2 LITTLE BLUE RIVER BRIDGE

The Little Blue River Bridge is a three-span bridge built in 1976 using elements from several salvaged bridges (Szerszen et al., 2019). The bridge consists of two plate girder approach bridges in the first and the third spans and a truss bridge in the middle span. The middle span was selected for load testing because it is a unique section that will likely have an unexpected torsional response. The initial inspection, shown in Figure 4.1, revealed some corrosion, deterioration, and deformation on parts of the truss and deck. The

section and damaged members should lead to complicated deflection results that would be hard to monitor using traditional methods or predict using a FEM model.

(a) (b)

Figure 4.1: Bridge S005 00446 condition: (a) truss and (b) deck (courtesy of Szerszen et al., 2019).

4.2.1 BRIDGE INFORMATION AND INSTRUMENT SETUP

The specifications of the Little Blue River Bridge are given in Table 4.2, with emphasis given to the scanned middle truss span, which was deemed to be the most concerned span and chosen for detailed monitoring. The 190.5 cm thick open grate steel grid is supported by nine W30x108 interior steel stringers as shown in Figure 4.2. Figure 4.2 also gives the type 3 triaxial truck (222.4 kilonewtons (kN)) position for the center and offset LL scans as well as the scanner location during both of those scans. The scanner was placed very close to the center of the span to limit the impact of the angle of incident and distance on the accuracy of the point cloud. The truck shown in is facing south and is positioned where the middle tire is placed at the midspan of Figure 4.3 the bridge, which is approximated as the worst-case loading.

Table 4.2: Bridge information summary for bridge S005 00446.

Bridge ID	S005 500446	**Span 2 Type**	Steel Pony Truss
County	Thayer	**Span 2 Deck Type**	Open Grate Steel Grid
Year Build	1976 using elements from salvaged bridges	**Span 2 Deck Thickness (cm [in])**	190.5 [7.5]
No. of Spans	3	**Stringer Shape**	W30x108
Length Span 1 (m [ft])	18.90 [62]	**No. of Interior Stringers**	9
Length Span 2 (m [ft])	30.48 [100]	**Stringer Spacing (cm [in])**	3048 [120]
Length Span 3 (m [ft])	18.90 [62]	**Top Chord Shape**	Two C10x20
Bridge Width (m [ft])	9.60 [31.5]	**Bottom Chord Shape (depends on location)**	Either two C10x20 or two C10x35
Skew Angle (°)	0	**Vertical and Diagonal Shape**	W10x45

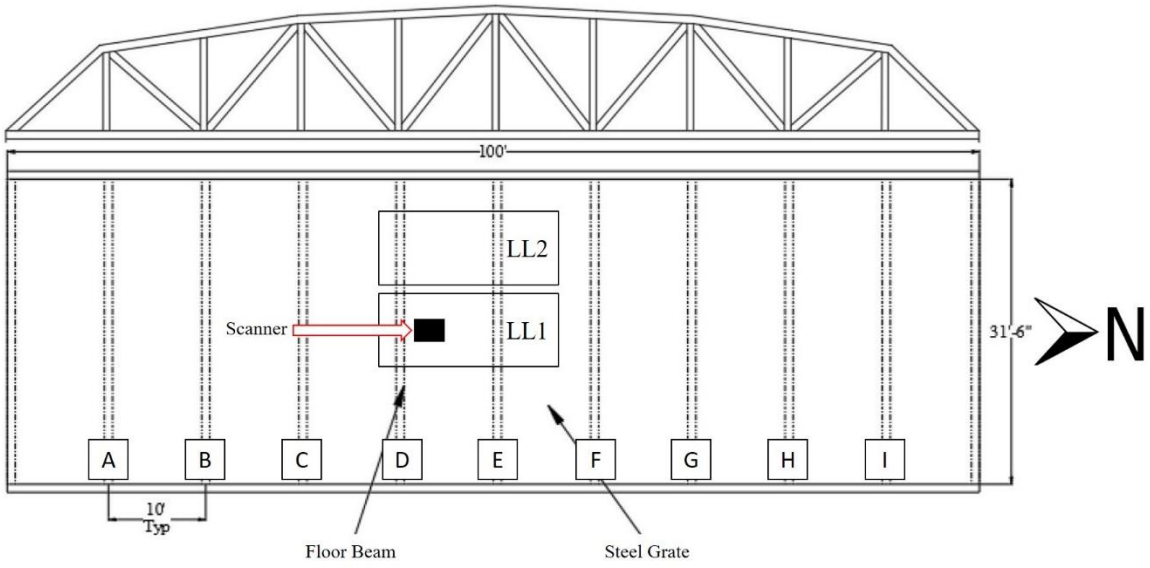

Figure 4.2: Top view of the general plan for bridge S005 00446 for span 2 (1 foot = 0.305 meters) (courtesy of Szerszen et al., 2019).

Figure 4.3: Photo of center load case for bridge S005 00446.

4.2.2 RESULTS DISCUSSION

The two LL point clouds created from the lidar scans are aligned to the DL point cloud using point to point registration. Point to point registration aligns the scans by manually selecting points on the piers, which are assumed to deflect negligibly during the loading. Using the C2C distance tool outlined in Chapter 2.1, the DL only cloud is compared to the two LL clouds in the vertical or z-direction. The DL cloud is the reference point cloud to which the LL point clouds will be compared to find the deflection or distance between them. The C2C distances for the two load cases are shown in Figures 4.4 and 4.5. Blue represents the greatest vertical differential deflection between the DL only cloud and the DL plus LL clouds. For both load cases, the location of the truck corresponds to the greatest LL deflection. Note that these figures are shown from the point of view below the bridge. In addition to the C2C figures shown, a pier in the point clouds is segmented out to

determine the precision of the alignment via C2C distance computations. The pier is used to compute the distance because it is assumed its deflection is negligible during the loading. The pier segments produce mean distances of 0.21 and 0.41 cm for the center and offset LL, respectively, indicating the tightness of the lidar registration. Note that the corresponding measured standard deviations are 0.10 and 0.15 cm.

A 1 cm section of stringer E was then segmented out and plotted as Figures 4.6 and 4.7 comparing the DL only point clouds with the two LL point clouds, respectively. Figures 4.6 and 4.7 are oriented along the section cut shown in Figures 4.4 and 4.5, with start representing 0 cm for the cross-section and end representing approximately 950 cm. Note the point clouds appear noisy, especially between 350 and 600 cm due to corrosion of the steel stringer causing a rough surface. The two figures display very different deflection results. Figure 4.6 appears to have a fairly constant deflection throughout, except close to the start when the LL case gets closer to DL only, signaling a slight rotation. This slight rotation is likely due to the truck not being placed exactly over the center of the span in the transverse direction. Figure 4.7 shows substantial deflection over the wheel lines, but on the opposite side, the LL case actually has upward deflection displaying a substantial amount of rotation. Figure 4.8 was created as another view of the LL deflection created from the center and offset LL, respectively. This was created by segmenting the stringer E cross-section into 100-cm increments and calculating the deflection by using a linear best fit line to calculate the elevation in the middle of the 100-cm increments. The center LL deflects the most in the middle with a value of -0.34 cm and the least on the side that slightly rotates with a value of -0.06 cm. The offset LL deflects significantly more reaching -1.05 cm while the other side deflects upward 0.07 cm.

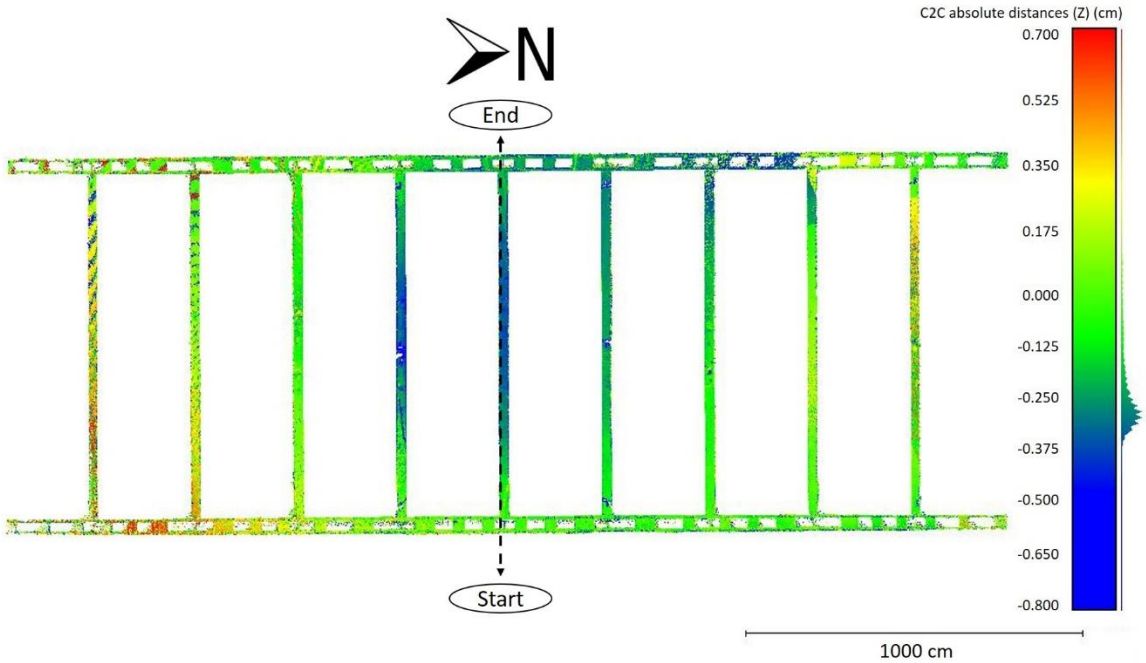

Figure 4.4: C2C distance between DL only and DL plus central LL (cm) (below the bridge viewpoint).

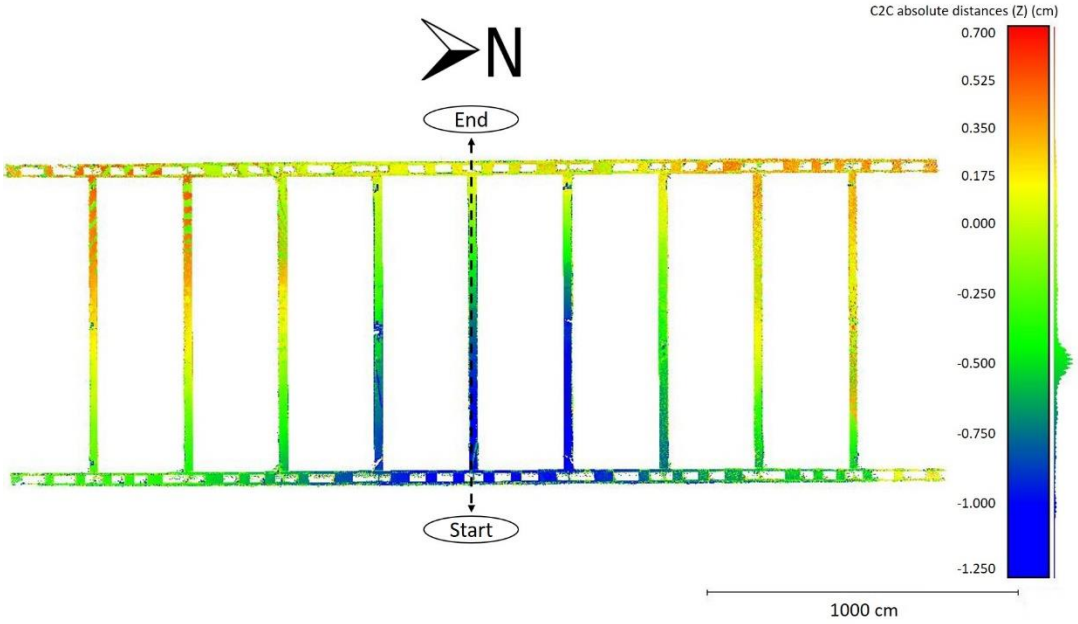

Figure 4.5: C2C distance between DL only and DL plus offset LL (cm) (below the bridge viewpoint).

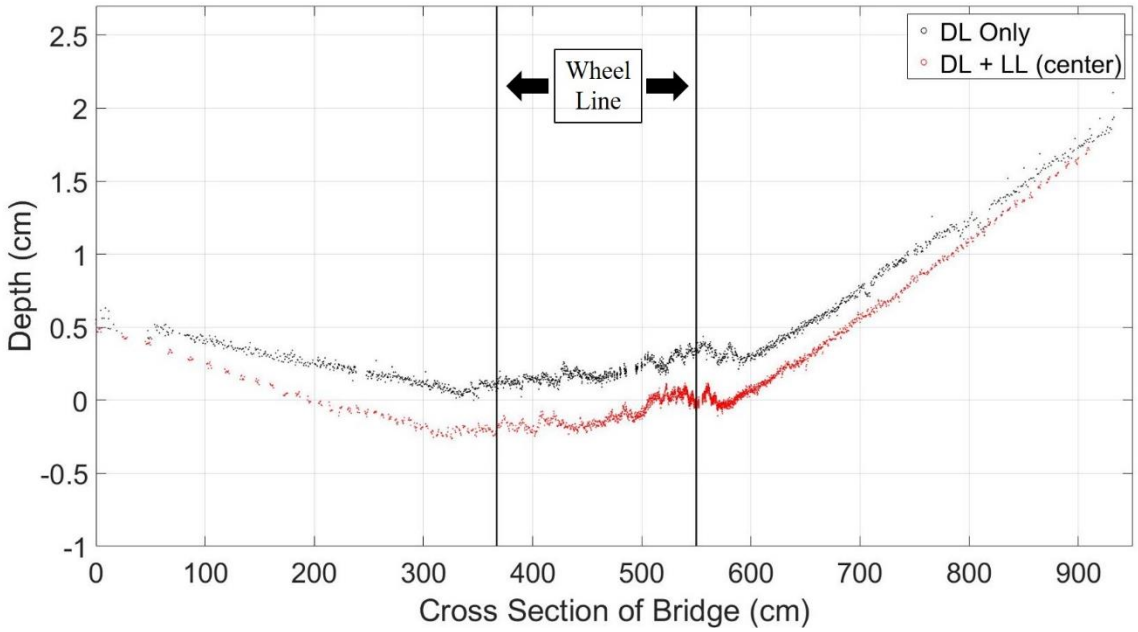

Figure 4.6: Stringer E depth: DL only versus DL plus central LL.

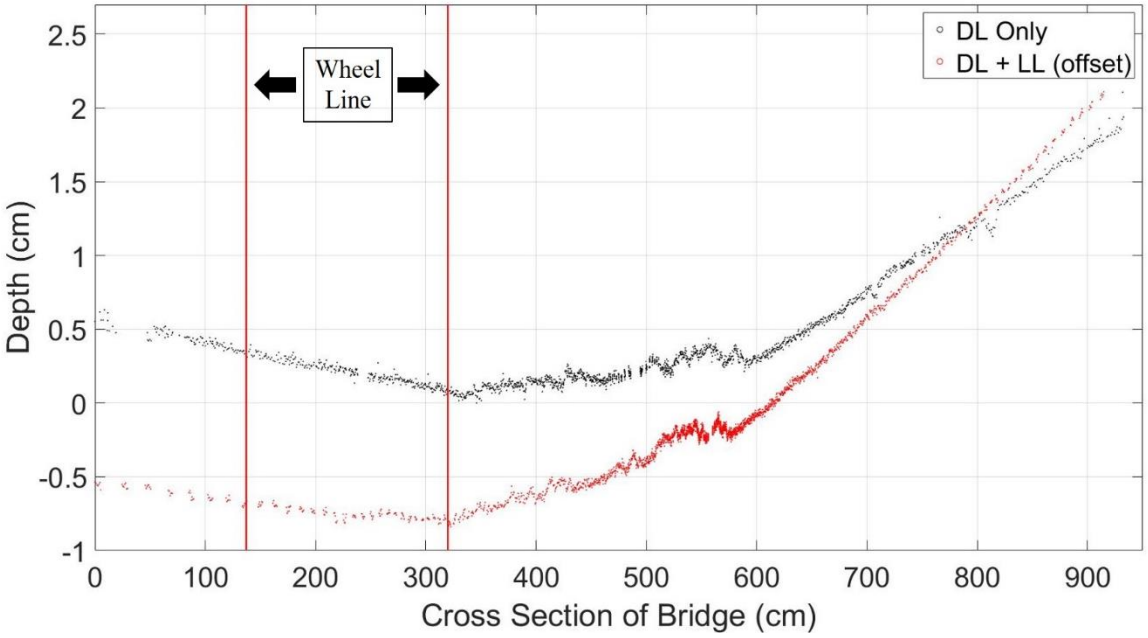

Figure 4.7: Stringer E depth: DL only versus DL plus offset LL.

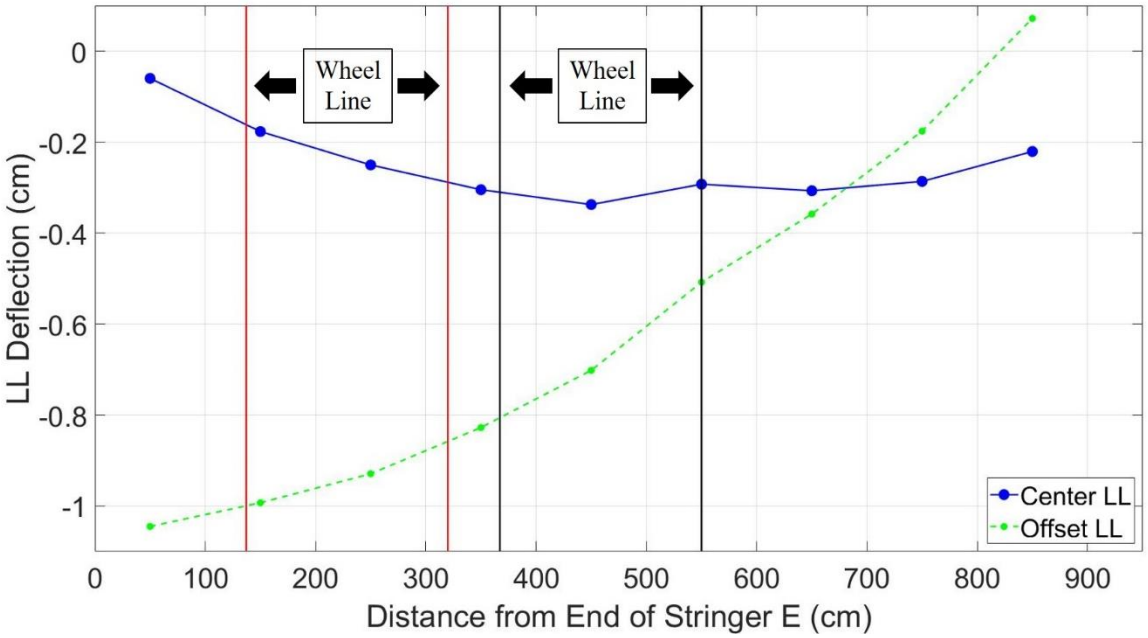

Figure 4.8: LL deflection at the midpoints of 100 cm intervals along stringer E.

4.2.3 KEY FINDINGS

The LL tests using the loaded triaxial truck for the Little Blue River Bridge display the stringers experience their largest deflections under LL near the wheel line of the truckload. Under the center LL, the bridge responds very uniformly, but under the offset LL the bridge undergoes substantial deflection near the wheel line but deflects upward on the opposite side. The bridge undergoes a considerable amount of rotation under the offset LL. The bridge-type creates an unexpected response, but can be used to validate and modify the FEM model.

4.3 BRUNSWICK BRIDGE

The Brunswick Bridge is a three-span bridge undergoing phased deck construction. The northbound lane is being replaced in phase I, and the southbound lane is being replaced in phase II. The existing girders and diaphragms will remain in place during the entirety of

the phased deck construction. As mentioned in Chapter 2.3, phased construction can lead to very unpredictable bridge responses that can cause costly and time-consuming fixes. The unpredictable nature of the phased construction could lead to complicated deflection results making it difficult to monitor using traditional methods.

4.3.1 BRIDGE INFORMATION AND INSTRUMENT SETUP

The Brunswick Bridge specifications are given in Table 4.3 and Figure 4.9, showing that the S014 17044 bridge consists of nine W24x68 steel girders. Figure 4.9 also exhibits that the scanner was placed near the middle of the northbound lane for the third span, where phase I construction was performed to mitigate the large incident angles and distance on the quality of the scans. A scan was taken before the deck was poured, immediately after the deck was poured, and sixty-six days after the deck was poured. The before scan was taken when no concrete was on the northbound lane, and the southbound lane was used for travel with the previously existing concrete. Then immediately after the deck was poured, a second lidar scan was collected after the concrete pour had finished. The concrete placement limit to the concrete pour is shown in Figure 4.10, which shows the pour for phase I is for exactly half the bridge width. Note after the concrete pour is completed, there will be a 122-cm gap between the fresh concrete of phase I and the existing concrete that will be removed for phase II. The scan taken sixty-six days later now has vehicles traveling on the northbound lane, whereas the southbound lane has the concrete removed. Figure 4.11 shows the construction crew pouring the deck for bridge S014 17044, and Figure 4.12 shows the underside of the bridge during the phase I deck pour. Note that the diaphragm spans the entire transverse direction.

Table 4.3: Bridge information summary for bridge S014 17044.

Bridge ID	S014 17044	**Phase I Construction Width (m [ft])**	6.50 [21.33]
County	Antelope	**Deck Thickness (cm [in])**	19.05 [7.5]
No. of Spans	3	**Girder Shape**	W24x68
Length Span 1 (m [ft])	10.26 [33.67]	**No. of Girders [Supporting Phase I]**	9 [5]
Length Span 2 (m [ft])	13.46[44.17]	**Girder Spacing: Interior 4 spaces (cm [in])**	158.75 [62.5]
Length Span 3 (m [ft])	10.26 [33.67]	**Girder Spacing: Exterior 2 spaces on each side (cm [in])**	137.16 [54]
Bridge Width (m [ft])	13.01 [42.67]	**Diaphragm**	Yes, but unknown dimensions
Skew Angle (°)	0		

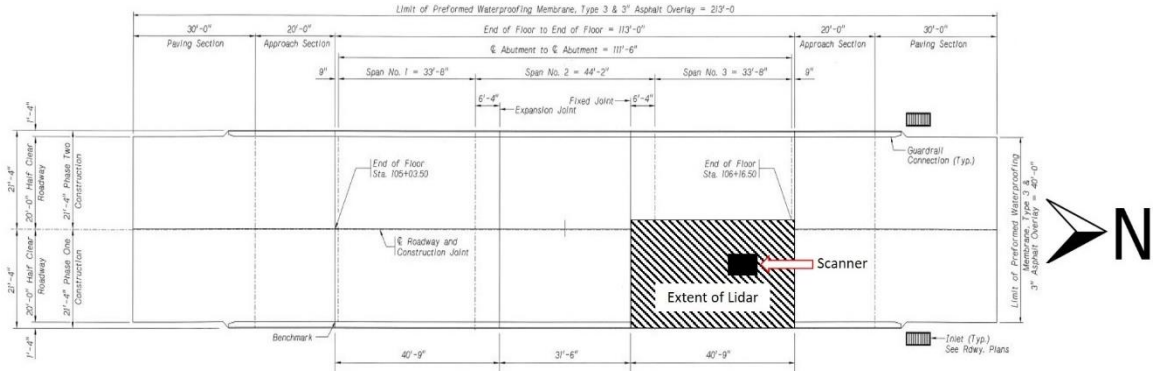

Figure 4.9: Top view of the general plan for bridge S014 17044 (courtesy of NDOT) (1 foot = 0.305 meters).

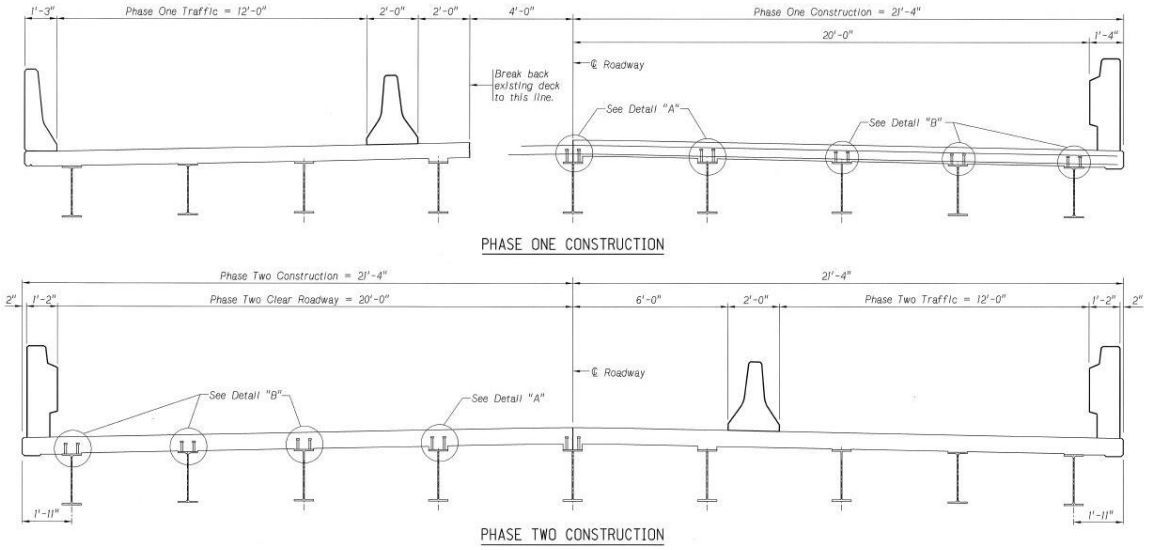

Figure 4.10: Phased construction for bridge S014 17044 (courtesy of NDOT) (1 foot = 0.305 meters).

Figure 4.11: Photo of deck pour for bridge S014 17044.

(a)

(b)

Figure 4.12: Photos underneath bridge S014 17044 during deck pour.

4.3.2 RESULTS DISCUSSION

The figures in this section will show the five girders involved in phase I construction. First, the two point clouds created from the lidar scans taken after the deck pour are aligned to the DL only point cloud. Point to point registration aligns the scans by manually selecting points on the abutment and pier. The abutment and pier are used because it is assumed their deflection is negligible during the loading. As outlined in Chapter 2.1, the DL only cloud is used as the reference scan to be compared to both of the deck pour clouds in the z-dimension. The C2C distances for both deck pour cases are shown in Figures 4.13 and 4.14, where blue represents the greatest vertical differential deflection. Note that these figures are shown from below the bridge point of view. In addition to these C2C figures, the pier for the point clouds is segmented out to determine the alignment precision using C2C distance computations. The pier is used because it is assumed to have negligible deflection during the loading. The pier segments produce mean distances of 0.21

and 0.21 cm for the immediate and sixty-six days after the deck pour, respectively, indicating the closeness of the lidar registration. Note that the corresponding measured standard deviations are 0.10 and 0.12 cm.

Similar to Chapter 4.2.2, Figure 4.15 was created by segmenting out cross-sections at midspan perpendicular to the girders where start represents 0 cm for the cross-section and end represents approximately 620 cm. Figure 4.16 was created by using linear best fit lines for each girder to find the phased deck deflection at the center of each girder. Note to reduce the error potential introduced by noisy or stray points, 5% of points were removed from each edge of the girder prior to linear fitting. Noisy edge points or edge artifacts occur primarily to beam scattering.

The figures show that the immediate deck pour deflection is greatest for the exterior girder and the smallest for the interior most girder while the intermediate girders are a fairly constant deflection between the two outliers. This is likely because the interior most girder only had concrete poured on half of it, so it had less mass to support. This resulted in a deflection of -0.04 cm compared to the intermediate girders which deflect between -0.12 and -0.13 cm. The exterior girder is deflecting the most to -0.20 cm. The greater deflection is likely due to it receiving less transverse support from the diaphragm because it is only being supported on one side and the Terex Bid-Well 2450 (26.9 kN) shown in Figure 4.11 is still located on the bridge when the after the pour scan was taken which increases the load placed on the exterior girder.

For the sixty-six days deflection, each girder sustained a significant increase in deflection. This can be attributed to creep, shrinkage, etc. as discussed in

Chapter 2.3.2. The interior girder remains the girder that deflected the least at -0.41 cm because it is only supporting concrete on one of its sides. The sixty-six days deflection differs because the greatest deflection now occurs at the second-most interior girder followed by the most exterior girder with values of -0.52 and -0.49, respectively. The second-most interior girder deflects the most at this time because it is the primary supporter of a temporary barrier, as shown in Figure 4.10. The exterior girder still will have less transverse stiffness than the interior girders and is now supporting a permanent barrier. However, the scaffolding and the Terex Bid-Well 2450 (26.9 kN), which can be seen in Figure 4.11 during phase I construction, were removed. This counteracts the mass that the permanent barrier added, resulting in the deflection for the exterior girder at this stage being predominantly from creep, shrinkage, etc.

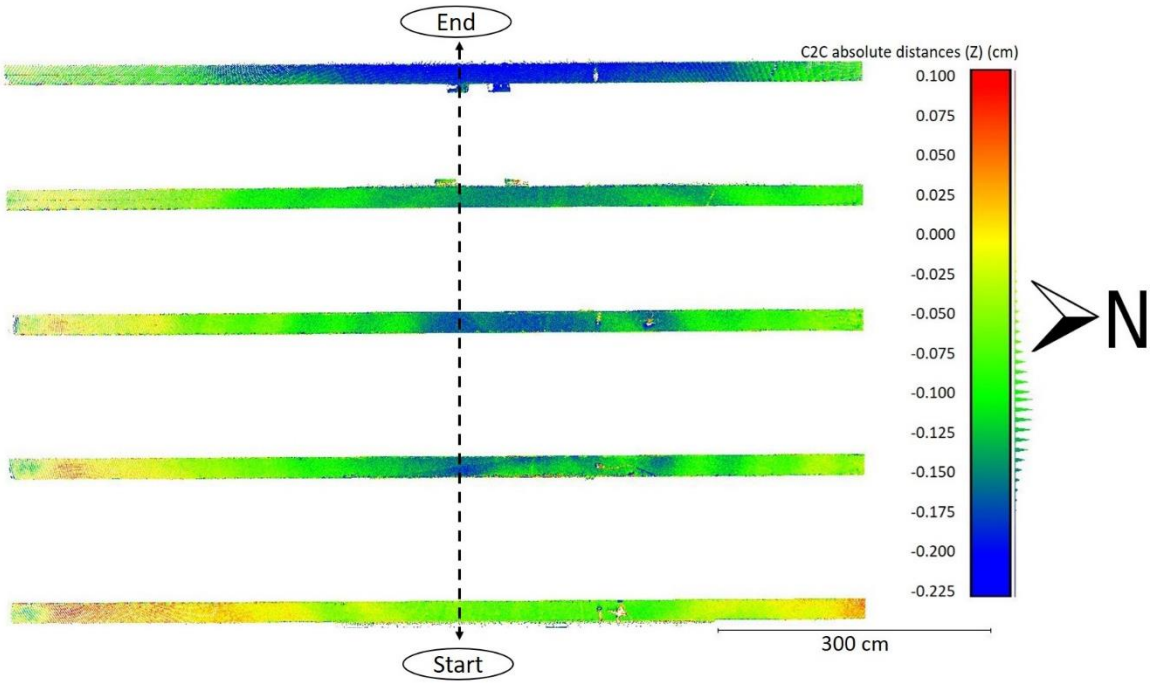

Figure 4.13: C2C distance between before and immediately after the deck pour (cm) (below the bridge viewpoint).

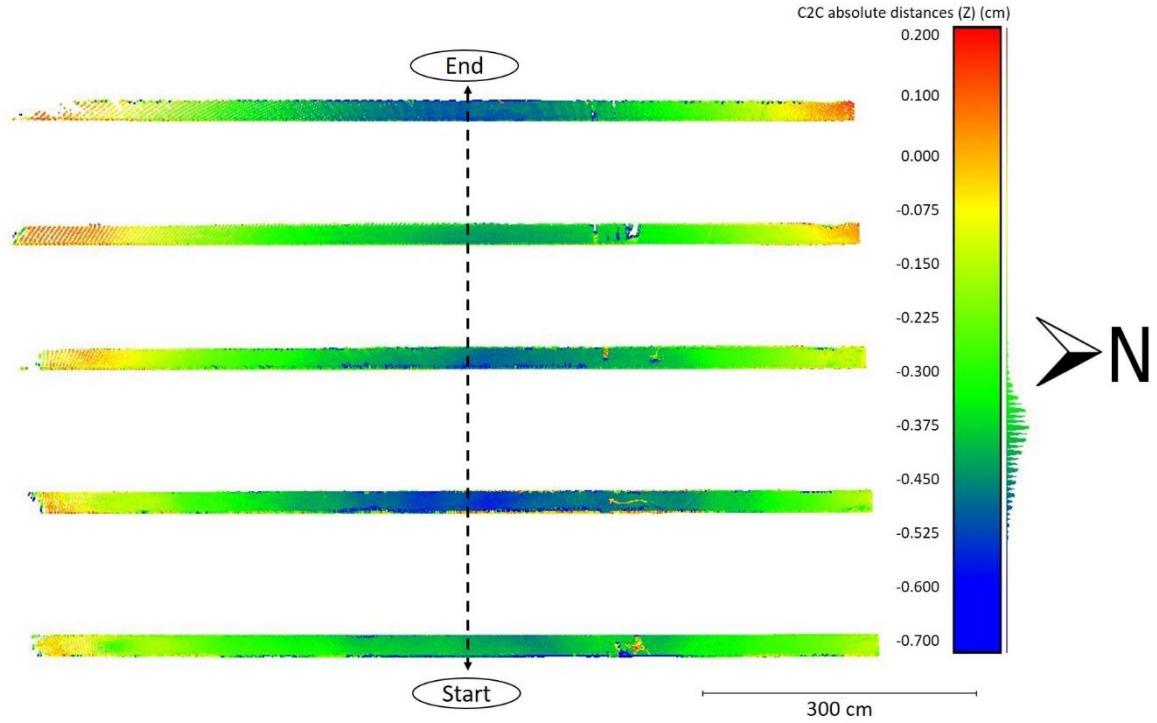

Figure 4.14: C2C distance between before and sixty-six days after the deck pour (cm) (below the bridge viewpoint).

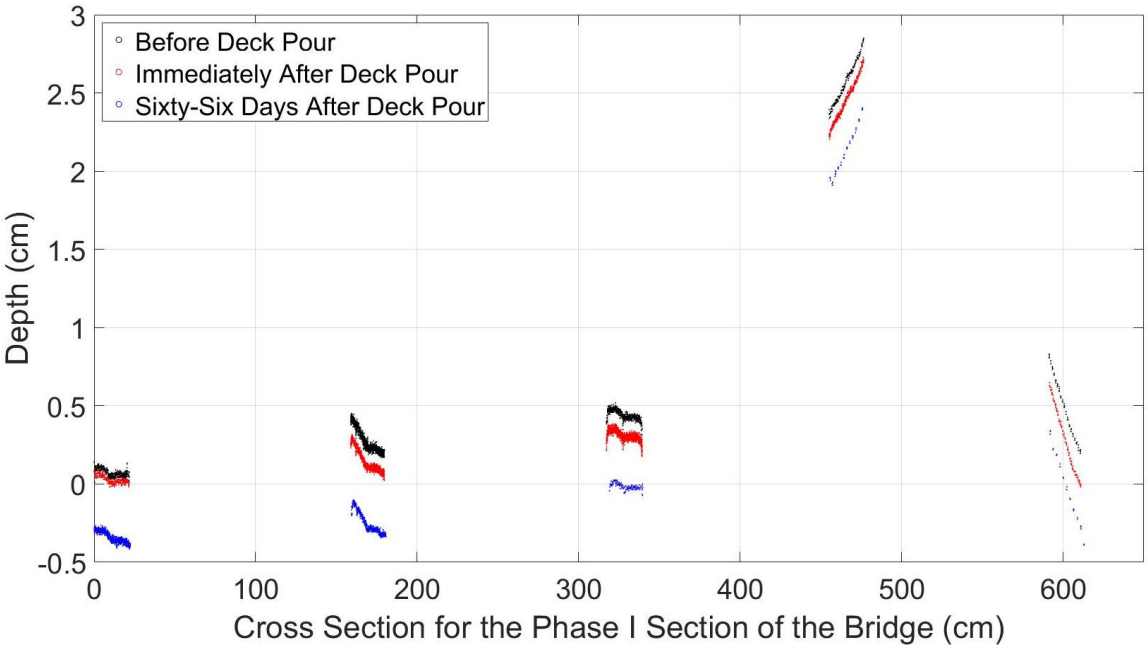

Figure 4.15: Girder depth at midspan perpendicular to the girders.

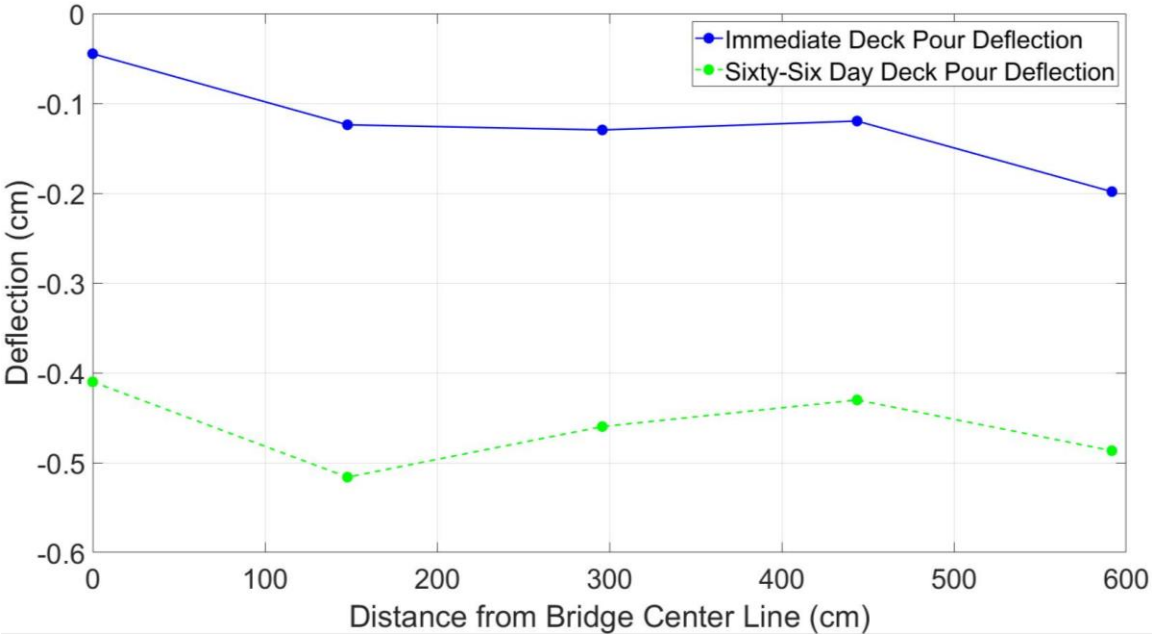

Figure 4.16: Deck pour deflection.

4.3.3 KEY FINDINGS

A few key findings for the phased construction concrete deck pour for the Brunswick Bridge can be made. The exterior girder deflected the most immediately after the deck pour likely due to lack of transverse stiffness and the extra mass of the Terex Bid-Well 2450 (26.9 kN), this is anticipated. The most interior girder deflected the least for both cases due to the least amount of mass from concrete. The second most interior girder deflected the most after sixty-six days due to the mass of the temporary barrier, once again as anticipated. Creep, shrinkage, etc. have a fairly uniform impact on the girders. Lidar was very effective at monitoring deflection at different stages of construction in a time and resource-efficient way. This includes the ability to distinguishes small changes in loads, as demonstrated by the temporary barrier. The unpredictability of short- and long-term

deflection would make final bridge properties difficult to predict from the design plans and if unaccounted for, may result in increased uncertainties in FEM models.

4.4 SILVER CREEK BRIDGE

The Silver Creek Bridge is a two-span bridge undergoing phased construction to replace the previous steel girders with IT-700 girders. The eastbound lane is being replaced in phase I, while the westbound lane is being replaced in phase II. Since the steel girders are being replaced by IT-700 girders, there will be no connecting diaphragm between the two phases of construction. This section will look at the short-term impact of a deck pour, which has previously been noted to have a non-uniform response which would be hard to predict via modeling (Martindale, Garret et al., 2019).

4.4.1 BRIDGE INFORMATION AND INSTRUMENT SETUP

The Silver Creek Bridge details are given in Table 4.4 and Figures 4.17 and 4.18 with an emphasis on the phase I construction. The specifications show that the S030 35969 bridge section of interest consists of ten IT girders while three steel existing girders will be supporting the traffic. Figure 4.17 also shows that the scanner was placed near the middle of the eastbound lane for the first span, where phase I construction will be performed. The placement reduces the impact of the angle of incident and distance on the point cloud accuracy. A scan was taken before the deck was poured and immediately after the deck pour was finished. The first scan was taken when no concrete was on the eastbound lane, and the westbound lane was a travel lane with the previously existing concrete supported

by the steel girders. The second scan was taken the same day once the concrete finished being poured. Figure 4.19 shows the construction crew pouring the deck for bridge S014 17044, and Figure 4.20 shows that shoring was added on the exterior two and a half girders. Additionally, there is a midspan diaphragm connecting the exterior three girders on both sides of phase I. The shoring and diaphragms are added to try to limit the deflection on the exterior girders caused by construction, which is a known issue for the IT bridge system (Martindale, Garret et al., 2019).

Table 4.4: Bridge information summary for bridge S030 35969.

Bridge ID	S030 35969	**Phase I Construction Width (m [ft])**	8.33 [27.33]
County	Merrick	**Deck Thickness (cm [in])**	15.2 [6]
No. of Spans	2	**Girder Height (cm [in])**	70.0 [27.56]
Length Span 1 (m [ft])	19.81 [65.00]	**Girder Width (cm [in])**	60.0 [23.63]
Length Span 2 (m [ft])	19.81 [65.00]	**Girder Spacing (cm [in])**	88.9 [35]
Bridge Width (m [ft])	14.23 [46.67]	**No. of Girders [Supporting Phase I]**	16 [10]
Skew Angle (°)	0	**Diaphragm**	C12x30

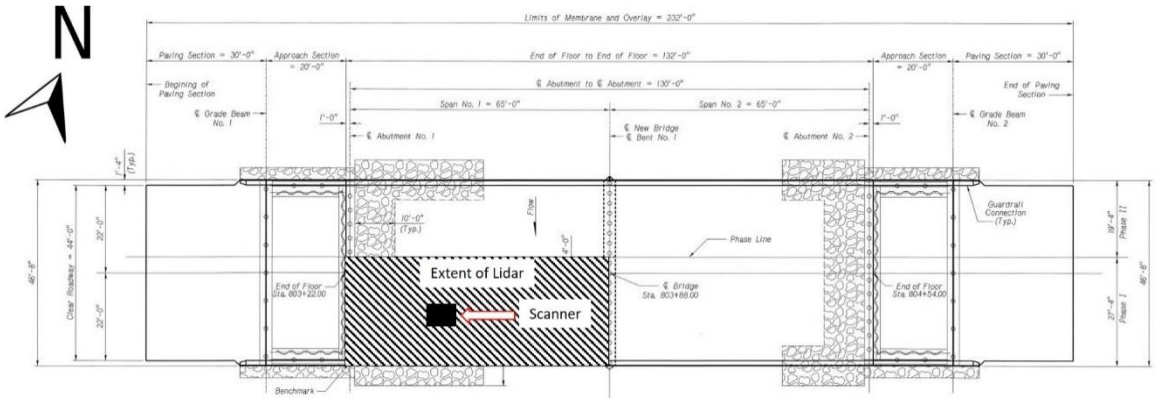

Figure 4.17: Top view of the general plan for bridge S030 35969 (courtesy of NDOT) (1 foot = 0.305 meters).

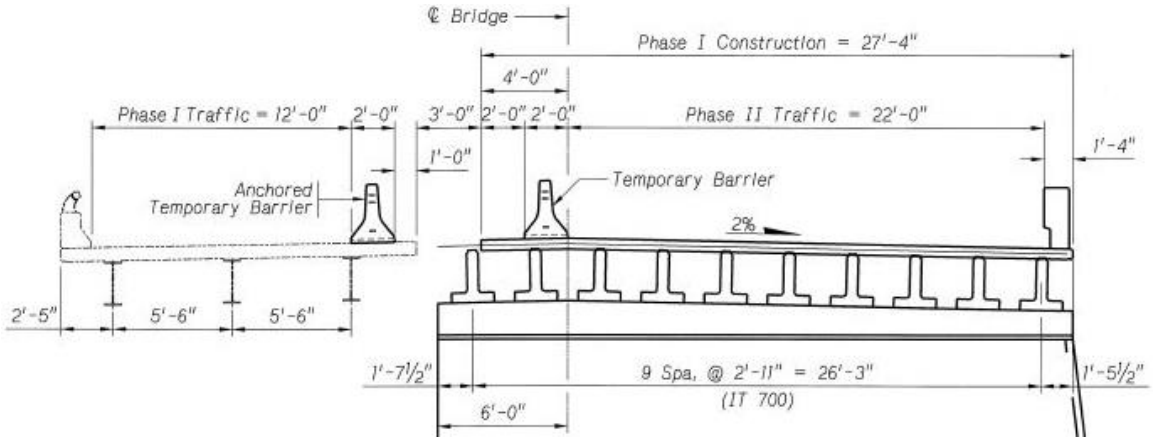

Figure 4.18: Phased construction for bridge S030 35969 (courtesy of NDOT) (1 foot = 0.305 meters).

Figure 4.19: Photo of deck pour for bridge S030 35969.

Figure 4.20: Photo of shoring for bridge S030 35969 deck pour.

4.4.2 RESULTS DISCUSSION

The point cloud created from the lidar scan taken after the deck pour is aligned to the DL only point cloud using point to point registration by manually selecting points on the abutment and pier. The abutment and pier are used because it is assumed their deflection is negligible during the loading. As illustrated in Figure 4.21, the DL only cloud is used as the reference point cloud that is compared to the deck pour cloud in the z-dimension using C2C distances with blue representing the greatest vertical differential deflection. As in Chapter 4.3.2, Figure 4.22 helps to visualize the bridge response where the figure is shown from the viewpoint below the deck. Additionally, the abutments are segmented out for C2C distance computations to determine alignment precision. The abutment segments produce

a mean distance of 0.46 cm indicating the tightness of the lidar registration. Note that the corresponding measured standard deviation is 0.10 cm. The cross-sections were segmented out at midspan perpendicular to the bridge with start representing 0 cm for the cross-section and end representing approximately 850 cm. The individual girders were used for those midspan cross-sections and fitted with a linear best fit line as in Chapter 4.3.2 to find the deck pour deflection at the center of each girder. The deck pour deflection is shown in Figure 4.23.

Similar to the Brunswick Bridge, the exterior girder deflected the most to -1.27 cm and although in this case the interior girder is not connected to the other phase via a diaphragm, it also deflected the least to -0.63 cm. The interior girder deflected the least because as demonstrated in Figure 4.18, it is not supporting any concrete at the time. Most of the concrete the interior girder will support is to be added during phase II. This means the deflection that is occurring is because it is supporting the next two girders by transversely distributing loads via the diaphragm. This explains why the two girders adjacent to it also do not deflect as much as the rest of the cross-section. Those two girders deflected -0.78 and -0.87 cm whereas the middle four girders deflected between -1.02 and -1.11 cm. This concept can be applied to the exterior girders as well. The girder adjacent to the exterior girder is deflecting the second most to -1.14 cm because it is taking some of the load from the exterior girder which deflects the most to -1.27 cm. As discussed in Chapter 4.3.2, the exterior girder receives less transverse stiffness from the diaphragm because only one side is supported, and it is supporting the load from the Terex Bid-Well 2450 (26.9 kN) which is still on the bridge when the scan was taken. The middle four

girders are very close in deflection, with one being a little higher than the others. This could have been caused by uneven deck thickness, camber error, construction error, etc. but appears to be a relatively minor error and does not impact the other conclusions.

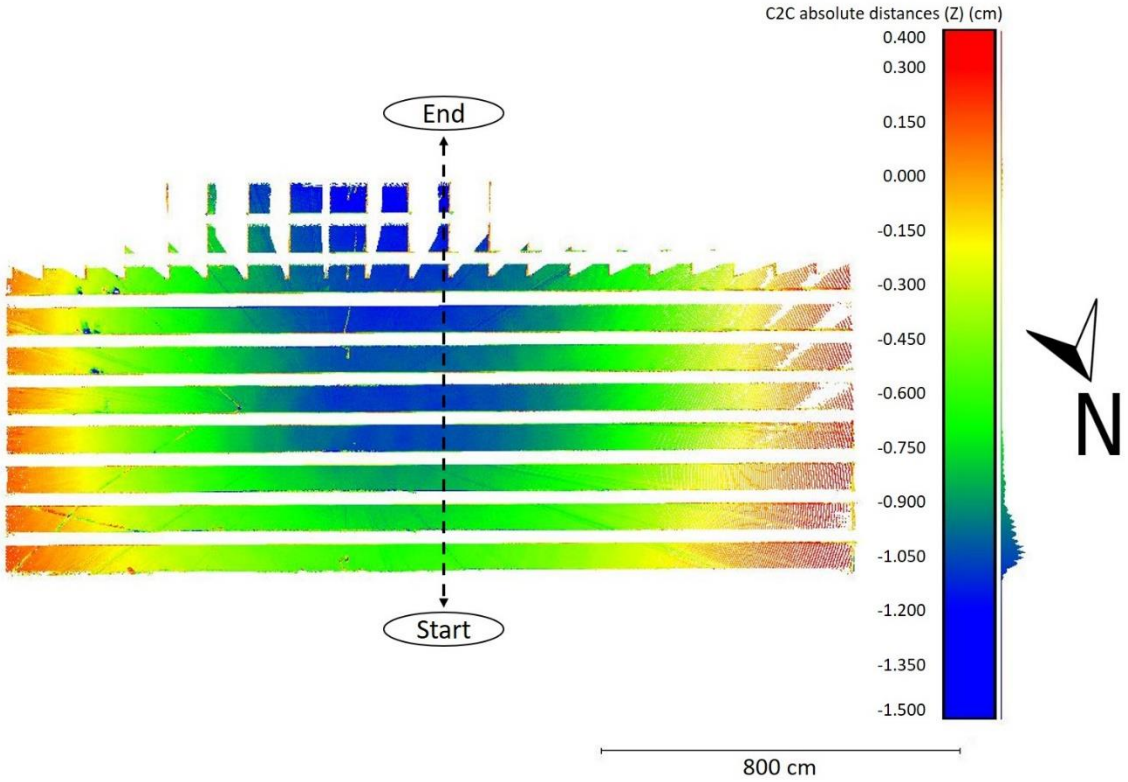

Figure 4.21: C2C distance between before and after the deck pour (cm) (below the bridge viewpoint).

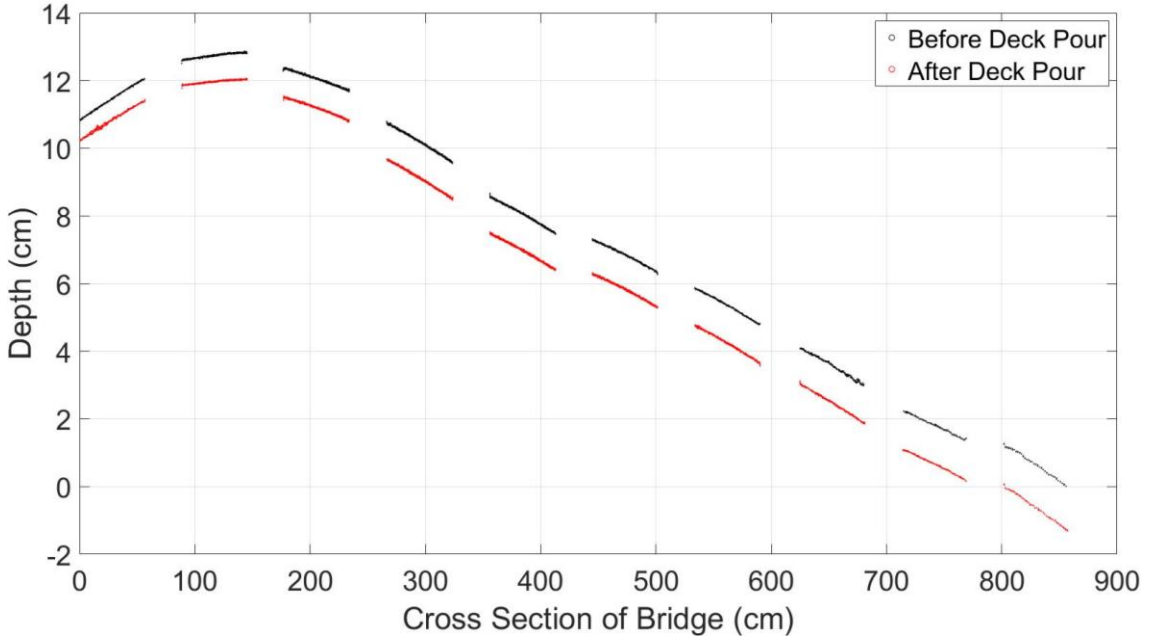

Figure 4.22: Girder depth at midspan perpendicular to the girders: before and after deck pour.

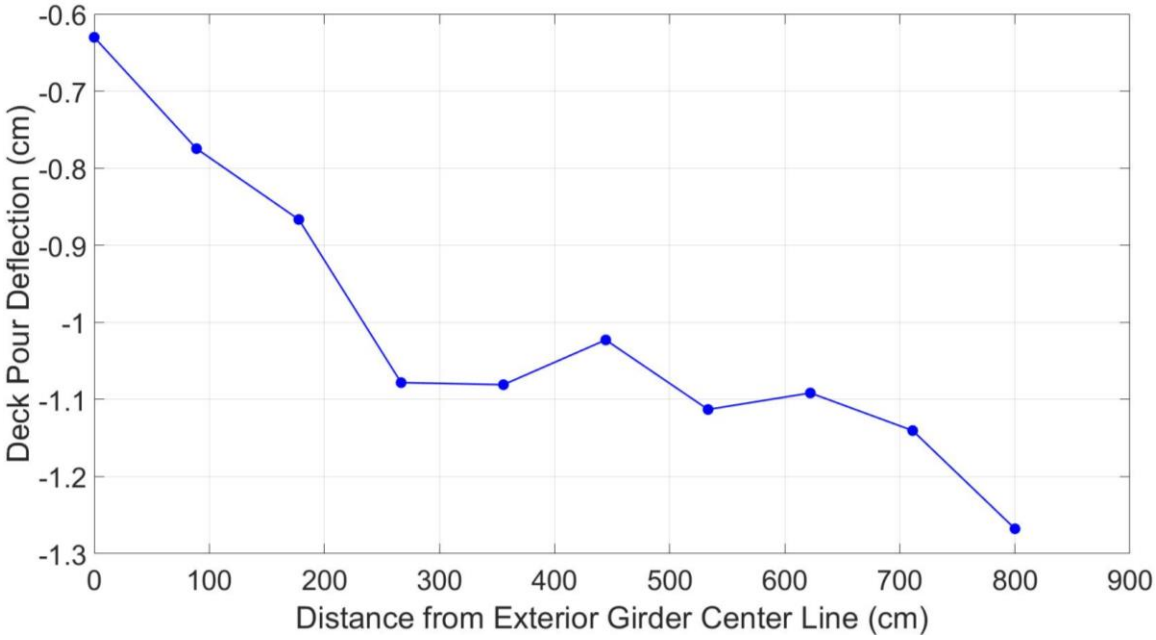

Figure 4.23: Deck pour deflection.

4.4.3 KEY FINDINGS

The phased construction concrete deck pour for Silver Creek shows that the most interior girder deflected the least due to not directly supporting any concrete, as anticipated. The interior girder provided transverse support to the adjacent girders via the diaphragm, causing those girders to deflect less than the middle girders. The extra mass of the Terex Bid-Well 2450 on the exterior girder causes it to deflect the most. The exterior girder received transverse support from the two adjacent girders via the shoring and the diaphragm, which made those girders deflect more. Lidar was able to capture a deflection that would be difficult to account for in a model. Calibrating with the lidar data will result in a better FEM model that will produce more accurate load ratings and distribution factors.

4.5 ELK CREEK BRIDGE

The Elk Creek Bridge is an IT girder bridge. Figure 4.24 displays the dimensions for the IT-600 girder used for the Elk Creek Bridge. The IT girder bridge system was originally developed in 1996 by the University of Nebraska–Lincoln (UNL) researchers and Nebraska Department of Transportation (NDOT) engineers (Jaber, 2013; Kamel & Tadros, 1996). The bridge system is considered as a type of accelerated bridge construction (ABC), which provides a competitive design for short to medium spans ranging from 9.1 to 24.4 meters. There are several advantages of the IT girder bridge system compared to other competitive systems. A few of the advantages include no required temporary formwork, quick construction process, shorter road closures, reduced bridge mass, and efficient material usage. The reduced girder mass increases the ease of construction for the

IT girder bridge system, especially for areas not easily accessible by large cranes. Also, the high span-to-depth ratio provides an adequate design for superstructure bridge replacements, especially when depth is a constraint (e.g., hydraulic clearance). However, this bridge system has been observed and noted in numerous bridge inspection reports to have extensive longitudinal and transverse deck cracking which is likely caused by a lack of lateral stiffness to transversely distribute the LL to all girders (Martindale, Garret et al., 2019; Martindale, Garrett P., 2018). The nonuniform and independent response of the girders likely will result in complicated deflection results that will be hard to monitor using traditional methods or predict using an FEM model.

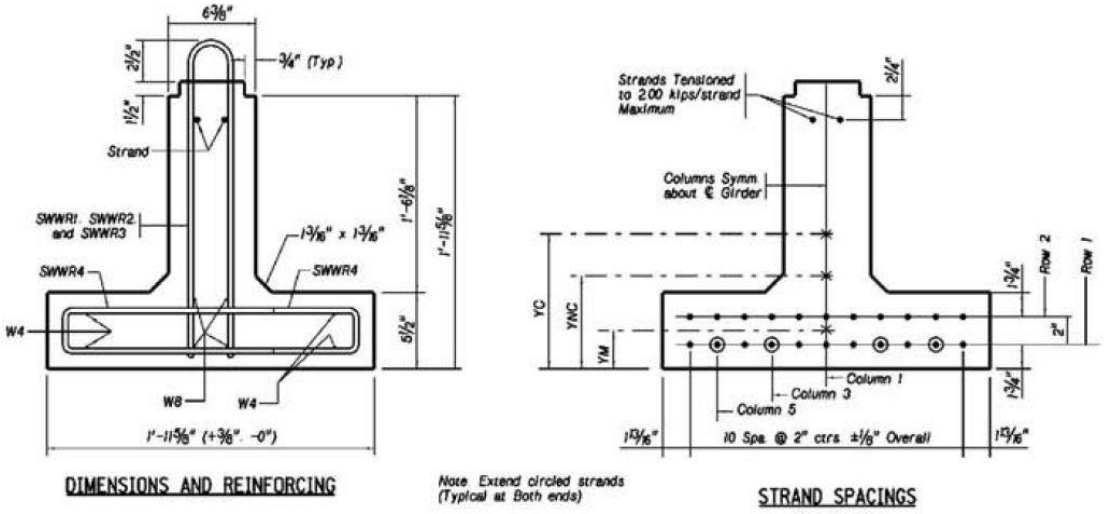

Figure 4.24: Drawing of the dimensions, reinforcement, and strand layout for a typical IT-600 girder (courtesy of NDOT) (1 inch = 2.54 centimeters).

4.5.1 BRIDGE INFORMATION AND INSTRUMENT SETUP

Table 4.5 and Figure 4.25 show that the C002408505 bridge consists of 13 IT-600 girders with a single 19.81-meter span. The general bridge plan is shown in Figure 4.25, while Figure 4.26 shows where the DL and LL scans were taken and where the type 3

triaxial truck (209 kN) was located for each LL scans. Notice that a scan for the DL case was taken at each end, but only one scan was taken for each LL scan. This was to limit the duration of time that the bridge was closed to traffic. The scans also could not be placed directly beneath the center of the span due to the creek. This will directly impact the quality of the point cloud on the opposite side of the scan because the angle of incidence and distance is increased. The two DL scans were aligned using ICP registration described in Chapter 2.1 and merged. ICP registration was utilized here because both scans were taken before loading, and therefore the bridge is not deflecting, and all points can be used for alignment. Figure 4.27 shows the truck position during the first load case. The first LL scan was with the triaxial truck placed on the center of the roadway while the second LL scan had the triaxial truck placed as close to the parapet as possible. The back tire of the center load case was 172.7 cm off-center facing in the south direction and the offset load was parallel to the girders because skew was unaccounted for when placing the truck.

Table 4.5: Bridge information summary for bridge C002408505.

Bridge ID	C002408505	**Girder Height (cm [in])**	60.0 [23.63]
County	Dawson	**Girder Width (cm [in])**	60.0 [23.63]
Year Built	2005	**Girder Spacing (cm [in])**	72.1 [28.38]
No. of Spans	1	**Deck Thickness (cm [in])**	15.2 [6]
Length Span (m [ft])	19.81 [65]	**No. of Girders**	13
Bridge Width (m [ft])	9.27 [30.4]	**Diaphragm**	C8x18.75
Skew Angle (°)	35		

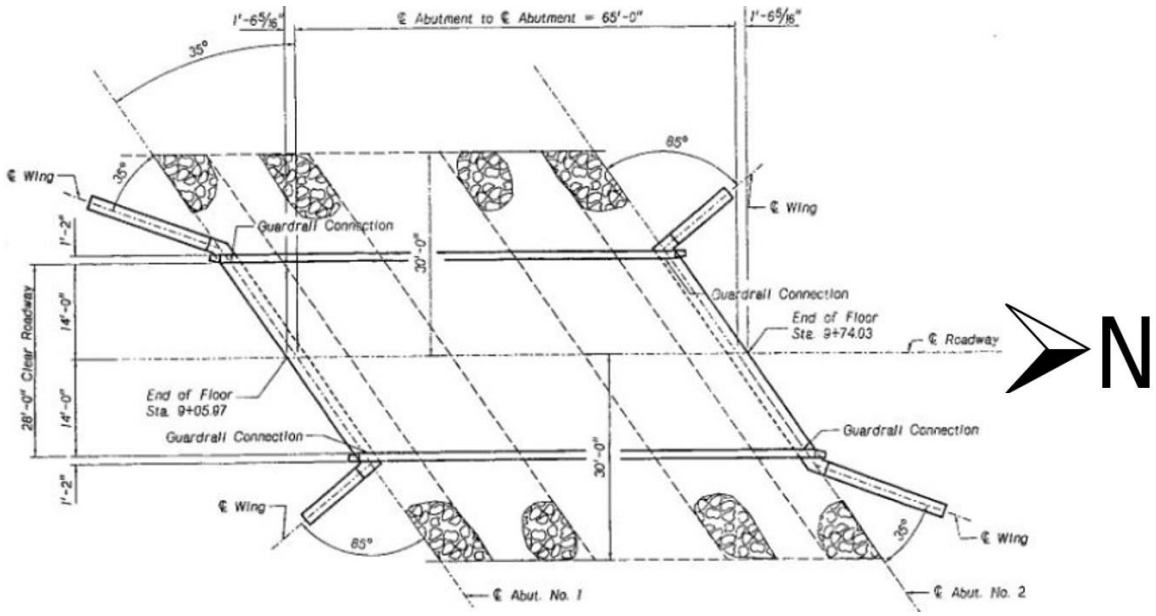

Figure 4.25: Top view of the general plan for bridge C002408505 (courtesy of NDOT) (1 foot = 0.305 meters).

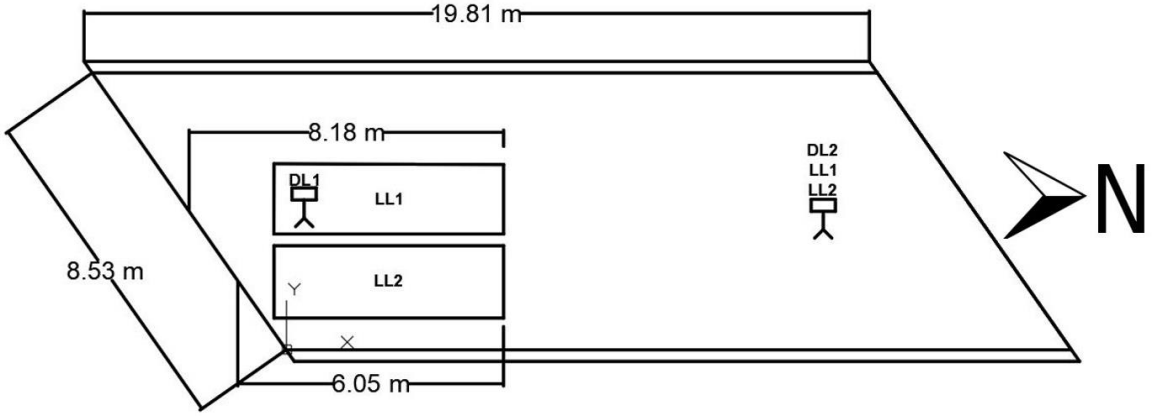

Figure 4.26: Laser scanner and truck locations for bridge C002408505.

Figure 4.27: Photo of center load case for bridge C002408505.

4.5.2 RESULTS DISCUSSION

The two point clouds created from the lidar scans taken while the triaxial truck was located on the bridge are aligned to the DL only point cloud. Point to point registration aligns the scans by manually selecting points on the abutments, which are assumed to have negligible deflection during the loading. The distance between the DL lidar generated point cloud and the DL plus LL point clouds can be calculated using the C2C distance tool outlined in Chapter 2.1. The DL only cloud is used as the reference cloud because it has a higher cloud density. The DL plus LL clouds will be the compared clouds meaning each of their points will be compared to the nearest point in the reference cloud by the vertical only. The C2C distances for the two load cases are shown in Figures 4.28 and 4.29 from a viewpoint below the bridge. Blue represents the greatest vertical differential deflection between the DL only cloud and the DL plus LL clouds. For both load cases, the location of the truck corresponds closely to the greatest LL deflection. The C2C distance

calculations on the segmented out abutment to determine alignment precision produce mean distances of 0.13 and 0.22 cm for the center and offset LL, respectively, indicating the compactness of the lidar registration. Note that the corresponding measured standard deviations are 0.08 and 0.14 cm. Figures 4.28 and 4.29 can be difficult to visualize, therefore, to obtain a better understanding of the deflection, cross-sections at midspan perpendicular to the bridge were segmented out with start representing 0 cm for the cross-section and end representing approximately 900 cm. These cross-sections were plotted as shown in Figures 4.30 and 4.31. These plots show the elevations of individual points in the DL only cloud and the DL plus LL clouds. Near the truck wheel lines, the girders deflect substantially but as they get farther away, the girders quickly return to the original undeformed elevation. The center LL deflected to a maximum of -0.26 cm versus -0.16 cm for the offset LL. The center LL deflected more due to the triaxial truckload being placed closer to the center span of the bridge.

To turn this deflection information into results that can be more easily compared, Figure 4.33 was made to show the LL deflections at the center of the girder. Figure 4.32 shows an example calculation for girder #8 under central LL. It shows that a linear best fit line was created using the data. In this equation, the arctangent of m is the girder rotation in radians and the relative midpoint depth is calculated by plugging in half the girder width in as x. Note that 5% of points were removed from each edge of the girder prior to linear fitting to reduce the error potentially introduced by noisy or stray points. These noisy edge points or edge artifacts happen primarily due to beam scattering.

The differential deflection between adjacent girders is shown in Figure 4.34. The max differential deflections occur just outside of the wheel lines with a critical max value of 0.076 for both load cases. Looking closely at Figures 4.30 and 4.31, it was noticed that the girders were not only deflecting, but they were also rotating. Figure 4.35 was created to display the differential in LL rotation. This is the change in radians of rotation between DL and DL plus LL for each of the girders. Over the section of loading, the girders go from clockwise rotation to counterclockwise rotation. The center LL caused a max rotation of 0.0011 radians counterclockwise the offset LL caused a max rotation of 0.0006 radians counterclockwise. The rotating of the girders may be slightly magnifying the differential deflection and may contribute to longitudinal deck cracking.

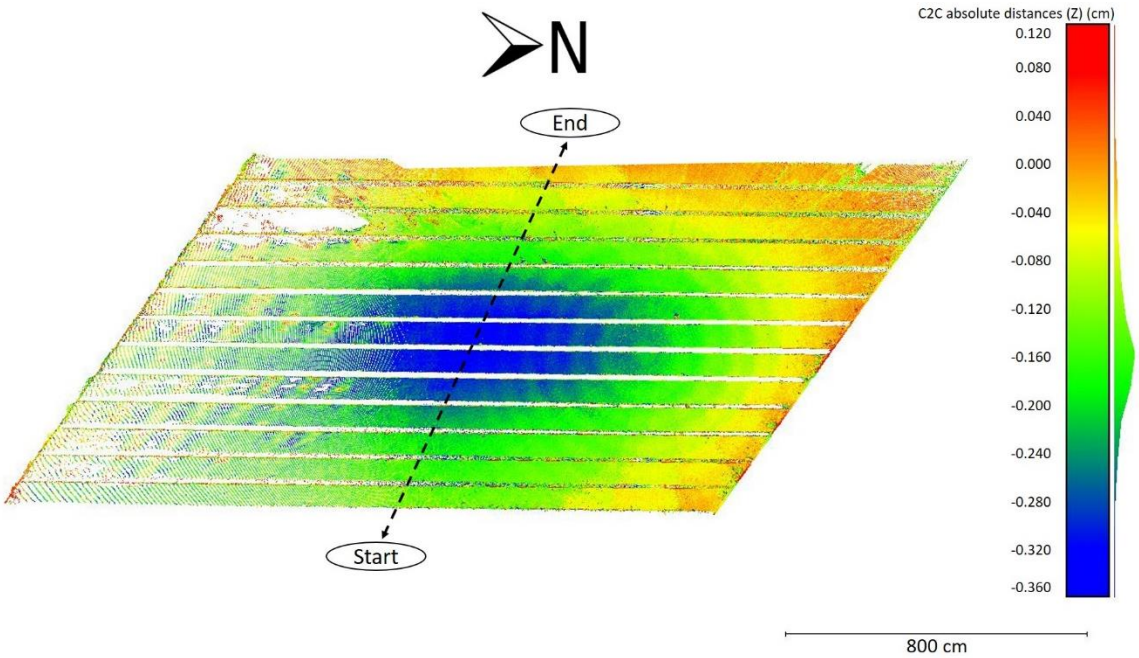

Figure 4.28: C2C distance between DL only and DL plus central LL (cm) (below the bridge viewpoint).

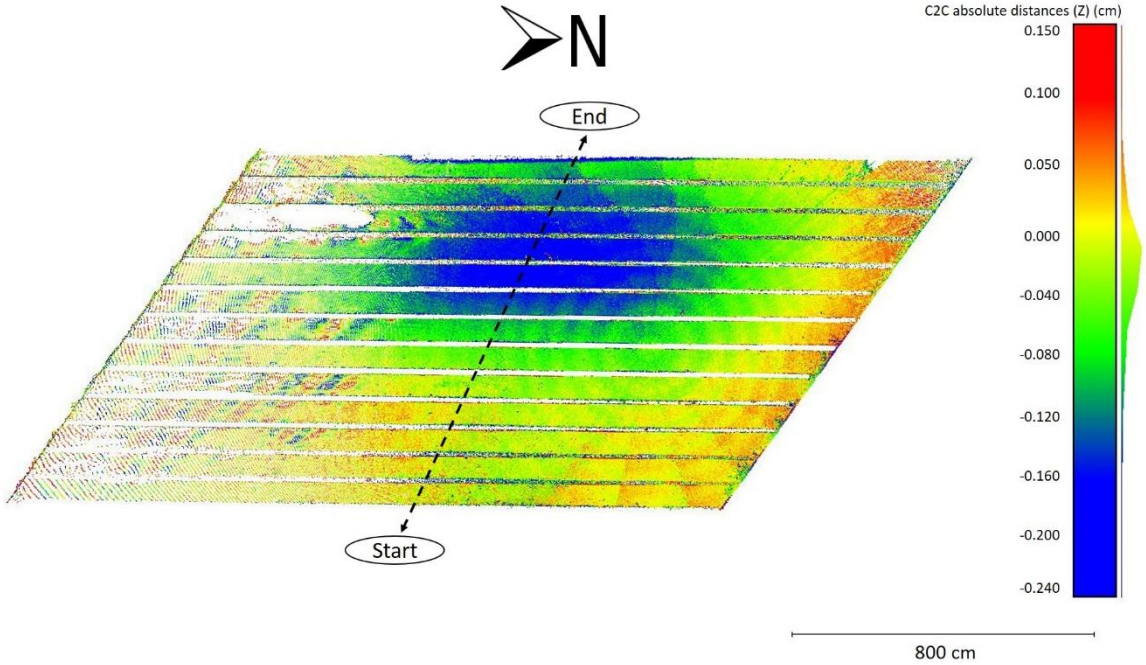

Figure 4.29: C2C distance between DL only and DL plus offset LL (cm) (below the bridge viewpoint).

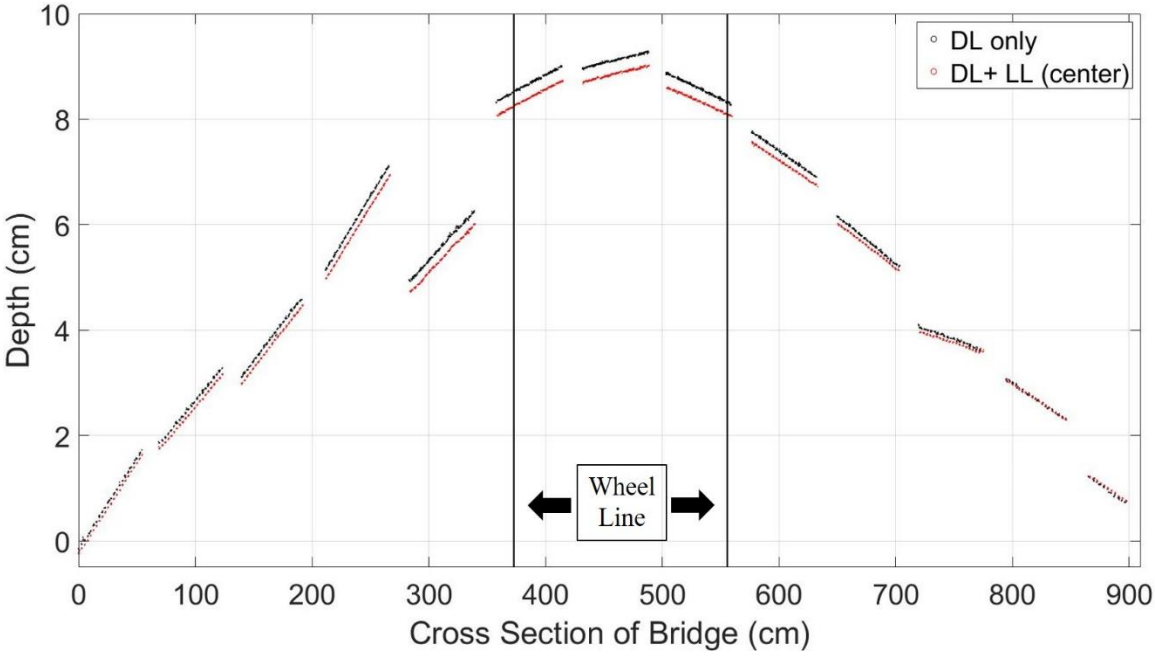

Figure 4.30: Girder depth at midspan perpendicular to the girders: DL only versus DL plus central LL.

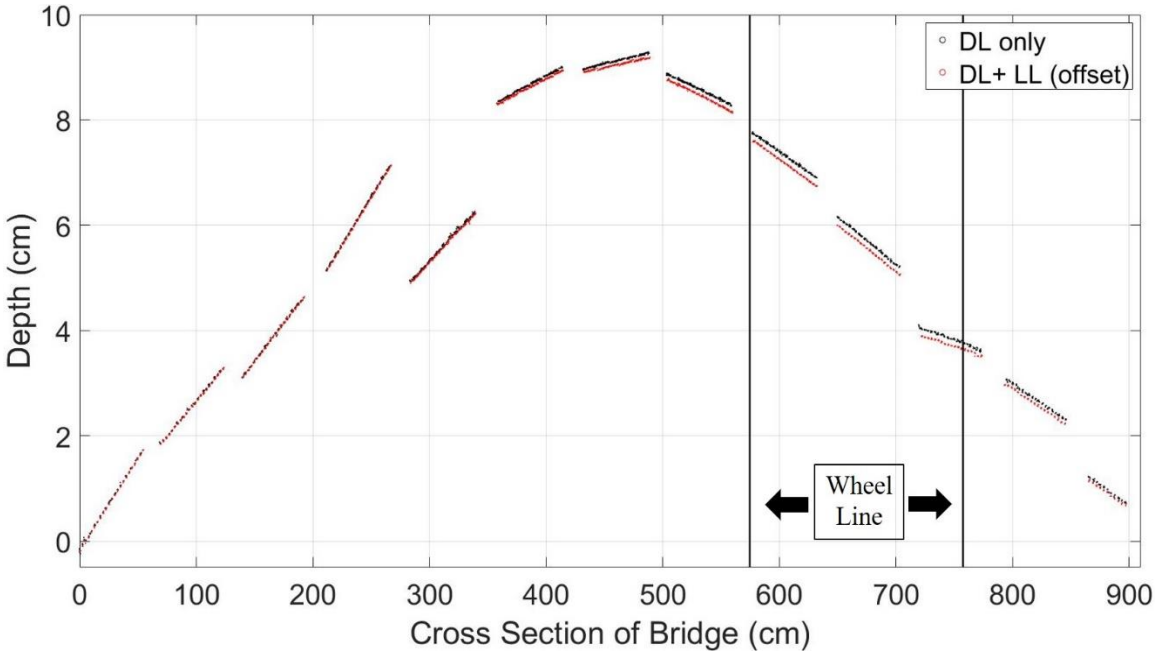

Figure 4.31: Girder depth at midspan perpendicular to the girders: DL only versus DL plus offset LL.

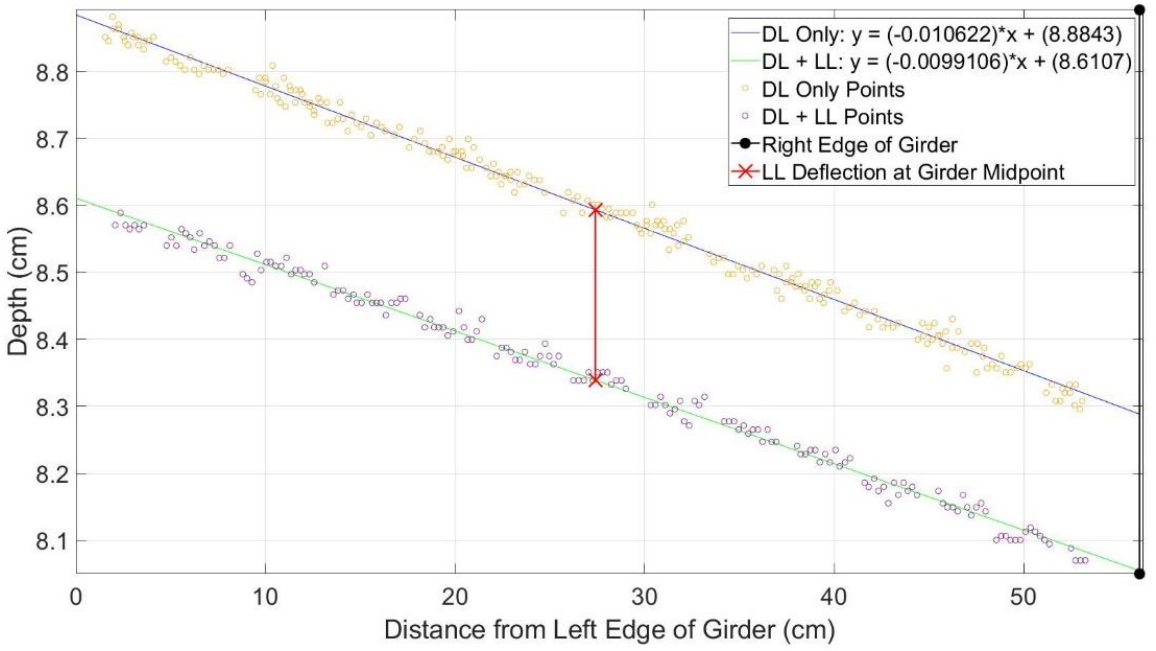

Figure 4.32: Example of calculations for girder #8 under central LL.

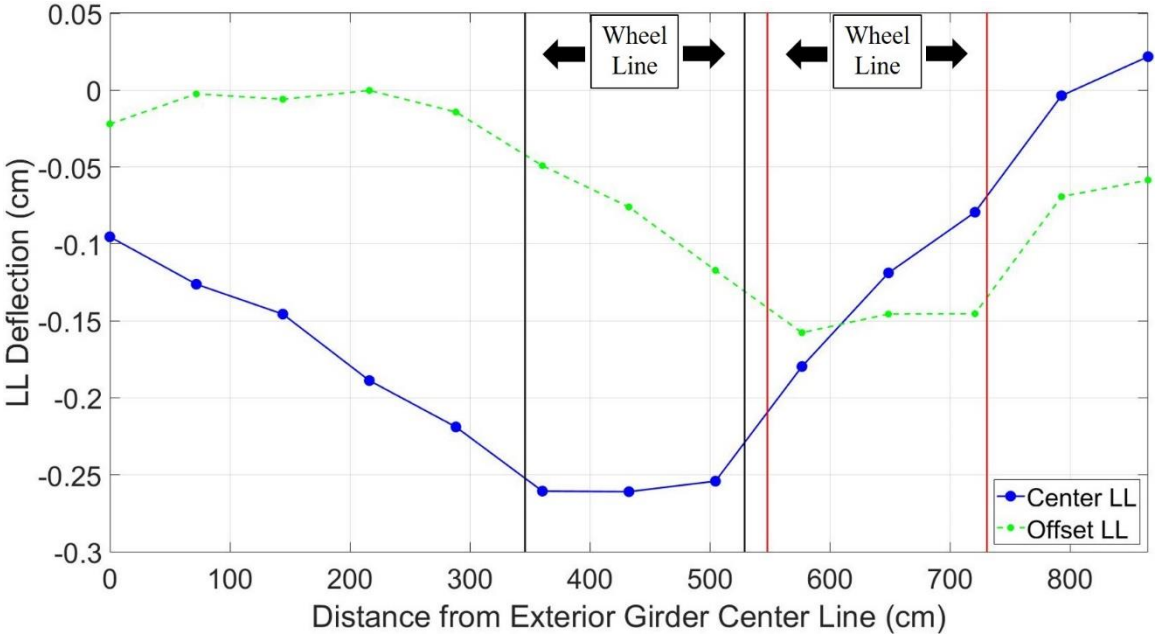

Figure 4.33: LL deflection at girder midpoints.

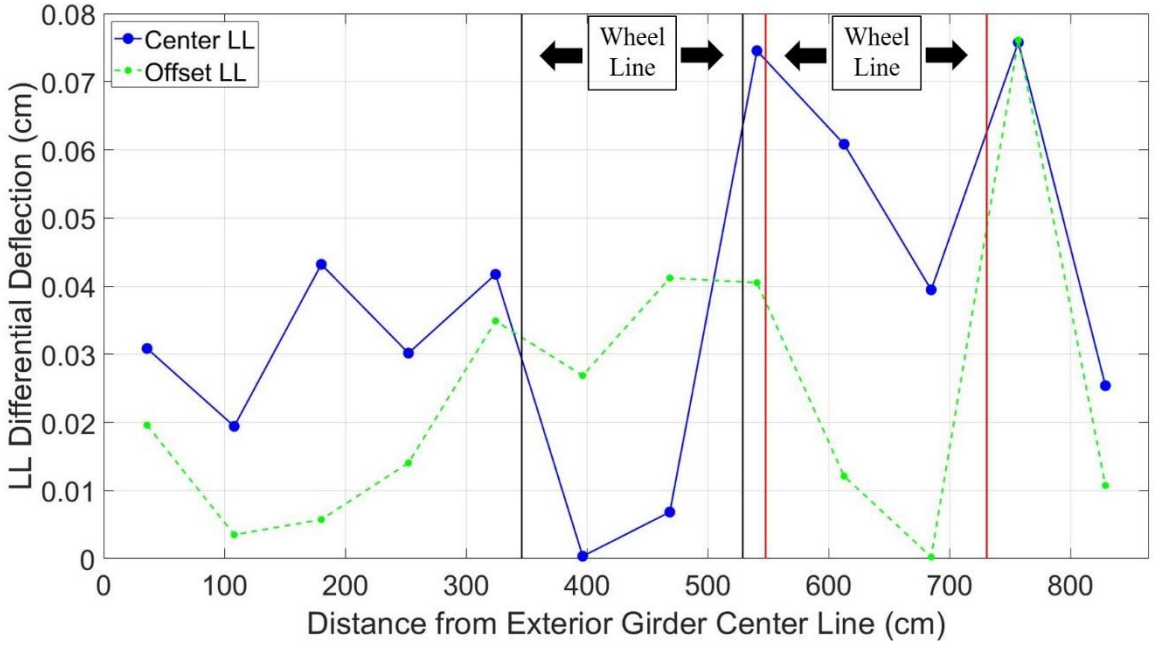

Figure 4.34: LL differential deflection between adjacent girders.

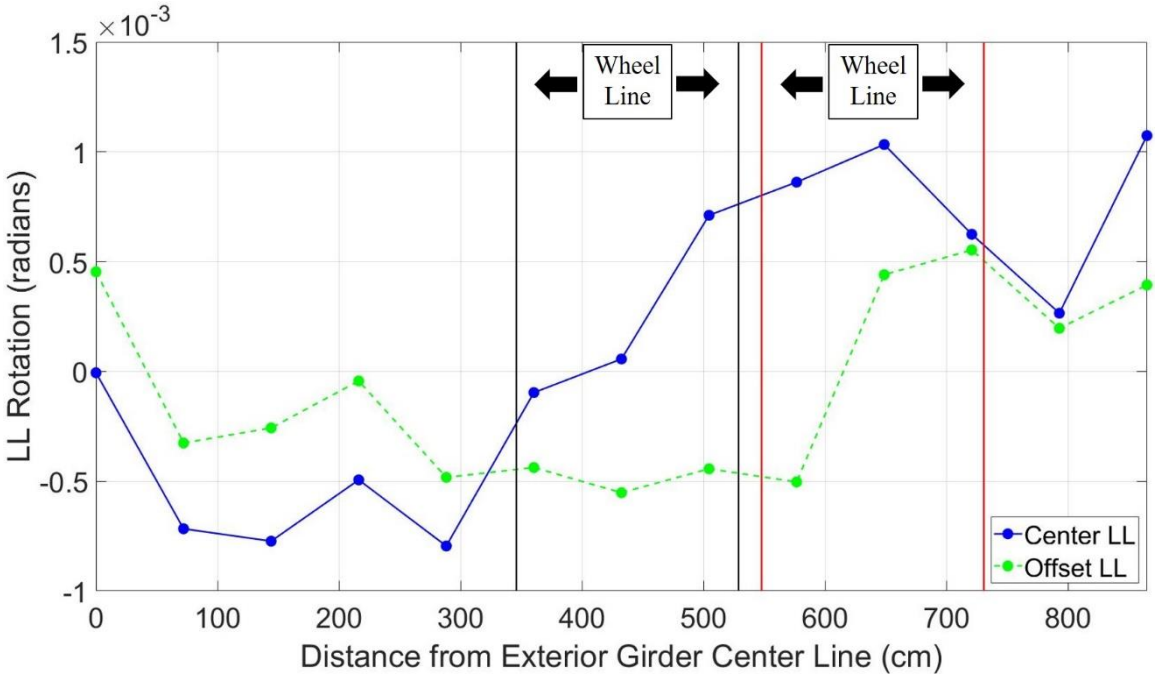

Figure 4.35: LL rotation of the girders.

4.5.3 KEY FINDINGS

The triaxial truck LL for the Elk Creek Bridge shows the girders experience noticeably larger deflections under LL where the wheel line is, but the deflection quickly reduces at adjacent girders. The differences in deflections between adjacent girders show that the girders are responding independently despite their narrow spacing, which may result in the longitudinal deck cracking in the IT girder bridge system. The girders are also rotating under LL, which may be contributing to longitudinal deck cracking.

4.6 OVERALL CONCLUSIONS

Based on all the bridge response tests, the following conclusions can be made. First, lidar was able to capture bridge responses such as unanticipated torsional response with a

high level of detail. Not accounting for these unexpected responses would produce inexact models that would lead to inaccurate load ratings and distribution factors. Using lidar data allows models to be calibrated to display the unintended torsional response that exists in real structures leading to more precise predictions. The capture of LL deflection and rotation by lidar can help identify problems in a structure such as the longitudinal deck cracking in the IT girder bridge system. Lidar was very effective at monitoring bridge response at different stages of construction, which is often a very difficult factor to predict. This may help give quick insight into fixing problems with phased construction in terms of camber and deflection.

CHAPTER 5 – NUMERICAL ASSESSMENT

5.1 INTRODUCTION

This section will summarize the use of CSiBridge to model the deflection of the Elk Creek Bridge described in Chapter 4.5. The model will be compared to lidar results to show the benefit of using lidar by displaying the response of a bridge response. These bridges have unexpected responses when undergoing LL and DL, which will make any numerical assessment difficult for precise modeling efforts. This is especially true when things such as the longitudinal deck cracking are being considered because the deck is less able to distribute loads transversely and in a less predictable fashion.

5.2 FEM MODEL DESCRIPTION

Bridge C002408505 was modeled in CSiBridge using the information summarized in Table 4.5 and Figure 4.25. CSiBridge was chosen for its ease of defining complex bridge geometries, boundary conditions, and load cases since it is specialized for bridge applications. The bridge uses shell elements for the deck, beam elements for the girders, and tendon objects for the prestressed tendons. The model was created using the deck and girder specifications in the design plans while increasing the compressive strength of the concrete to match the maximum deflection for the center load case. The compressive strength of concrete was used to calibrate the model based on the literature review in Chapter 2.2 which exhibited that f'_c is typically conservative. The 15.2 cm deck and IT-600 girders were modeled with compressive strengths of 44.8 and 62.1 MPa, respectively.

The loading was placed as it was in the field (Figure 4.26), where the back tire of the center load case was placed 172.7 cm off-center. The offset load was placed parallel to the girders because skew was unaccounted for when placing the triaxial truck. The weight of the loaded type 3 triaxial truck was at 209 kN total with the back four tires accounting for 34.9 kN each and the front two tires accounting for 34.7 kN, respectively. Tire spacings were 457 cm for the front-tire span and 122 cm for the back-tire span. The transverse tire spacing is 183 cm. The two models can be seen in Figures 5.1 and 5.2. Note that red represents the deck, and blue represents the girders and the diaphragm. In these models, x is pointing in the north direction and is parallel to the girders, y is in the west direction and is perpendicular to the girders, and z is pointing upwards to represent an increase in elevation.

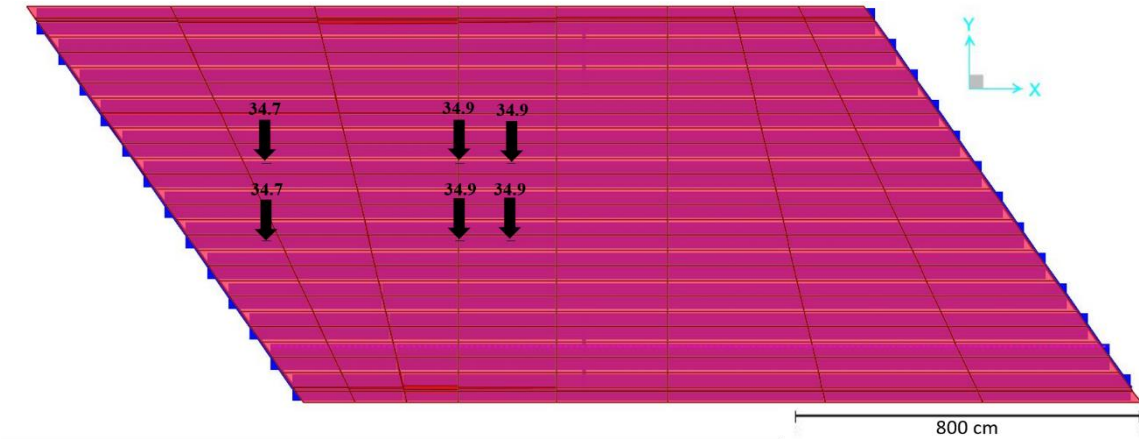

a)

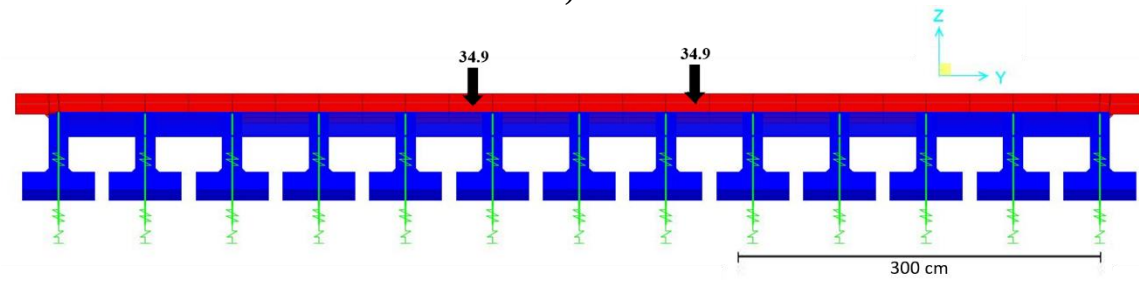

b)

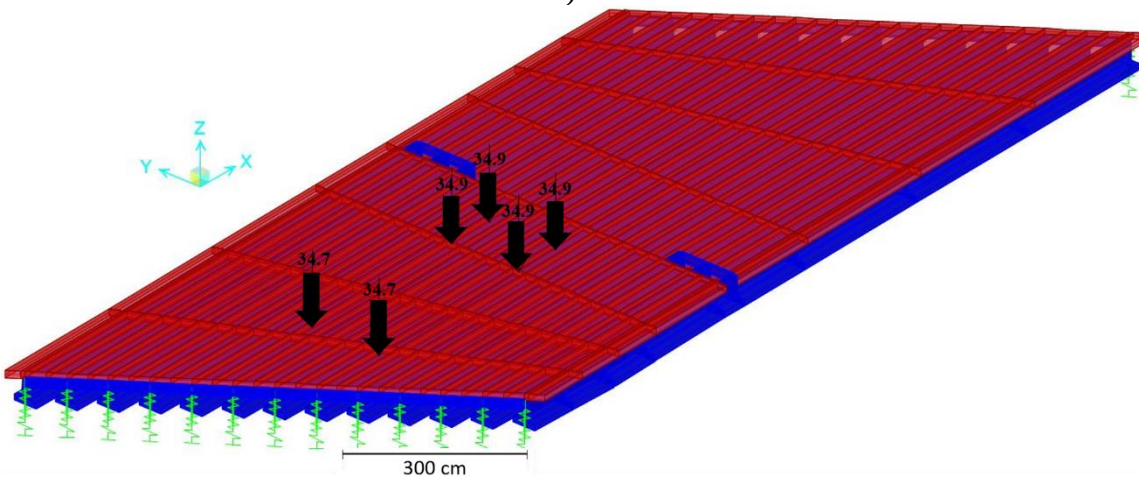

c)

Figure 5.1: CSiBridge model for center load case for bridge C002408505 for the a) top, b) side, and c) isometric view (load in kN).

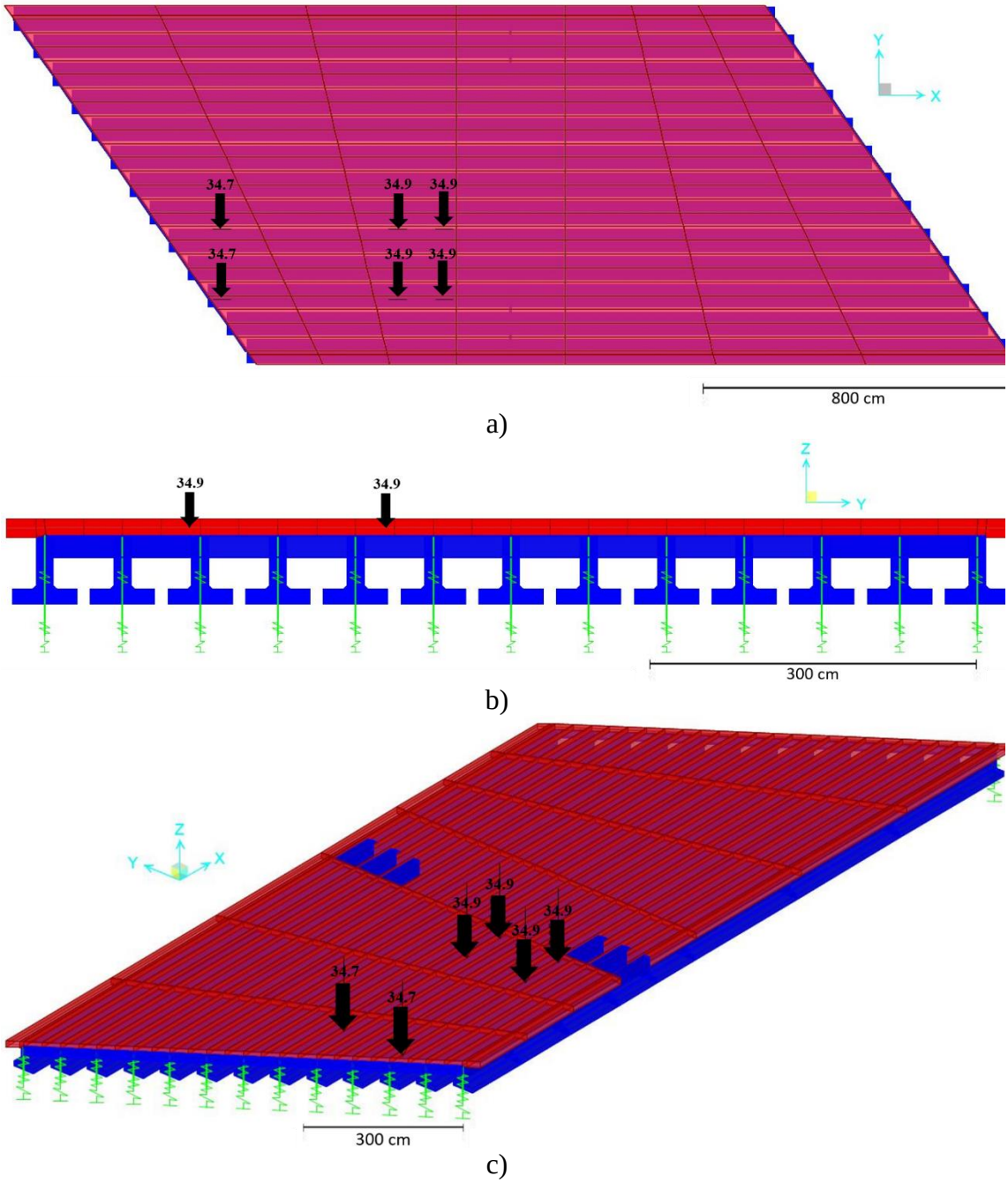

Figure 5.2: CSiBridge model for offset load case for bridge C002408505 for the a) top, b) side, and c) isometric view (load in kN).

5.3 DISCUSSION OF RESULTS

Figures 5.3 and 5.5 shows the FEM model deflection caused by the LL of the truckload for the center and offset LL from a viewpoint below the bridge, respectively. Dark blue represents the greatest vertical deflection caused by the truckload placement on top of the bridge, while red represents very little to zero vertical deflection. For both load cases, the location of the truck is very close to the spot of the greatest LL deflection and moves towards red near the abutments. The figures produced by the model can be compared to Figures 5.4 and 5.6, which were previously created from the lidar in Chapter 4.5.2. The figures from CSiBridge appear to be distributing the deflection in a more circular pattern than that of the lidar. This signifies a more uniform distribution of the load.

To make Figures 5.3 and 5.5 easier to visualize and better understand the deflection, the center girder deflections at midspan perpendicular to the bridge were segmented out with start representing 0 cm for the cross-section and end representing approximately 900 cm. These cross-sections and the cross-sections segmented out in Chapter 4.5.2 were plotted as shown in Figures 5.7 and 5.8. Both the lidar and the model has the greatest deflection occurring near the wheel line; however, the maximum values differ. For the center LL, the lidar deflects slightly more than the model with a value of -0.26 versus -0.24 cm. However, for the offset LL, the lidar deflects moderately more than the model with values of -0.22 versus -0.16 cm. These result in percent differences of 6.7% and 31.9% for the center and offset LL, respectively. The model also appears to have a much smoother, more uniform deflection with the girders far from loading experiencing greater deflection

than was measured in the field. This implies the model has greater transverse stiffness than the results from lidar.

The more uniform model predicted bridge response can also be seen in Figures 5.9 and 5.10, which shows the differential deflection between adjacent girders compared to the lidar results from Chapter 4.5.2. These figures emphasize the model producing significantly fewer differential deflections with values of 0.028 and 0.027 cm for the model as compared to 0.076 and 0.076 cm produced by lidar for the center and offset loadings, respectively. These result in percent differences of 92.1% and 94.7% for the center and offset LL, respectively. The differential deflection is important because as noted earlier, it is contributing to the longitudinal deck cracking observed in the IT bridge system. Also, note the max differential deflection of the model does not take place adjacent to the wheel lines as in the lidar but takes place two or three girders over. These figures help show how FEM models may have more trouble predicting the response for bridges with unique properties such as the IT girder bridge system.

To quantify the similarities between the cross-section deflections, an equation similar to the modal assurance criterion (MAC) was used. Although MAC is for modal analysis, it can still be used to quantify the difference between deformation shapes by comparing the similarities of two vectors. The equation is shown below as Equation 1, where $\{\varphi_X\}_q$ represents the first deformed vector, in this case either the center or offset LL lidar deflected shape and $\{\varphi_X\}_q$ represents the second deformed vector, in this case the corresponding FEM model. Values are bounded between 0 and 1, with 1 indicating a

consistent shape or a very similar deflection pattern and near-zero indicating not a consistent shape or a very different deflection pattern (Pastor, Binda, & Harčarik, 2012).

$$MAC\ (r,q) = \frac{|\{\varphi_A\}_r^T\{\varphi_X\}_q|^2}{(\{\varphi_A\}_r^T\{\varphi_X\}_q)(\{\varphi_X\}_q^T\{\varphi_X\}_q)} \quad (1)$$

Based on the deflection values in Figures 5.7 and 5.8, equation 1 was used to produce the quantitative analysis results. The FEM models both matched the lidar fairly well with values of 0.82 and 0.85 for the center and offset LL, respectively. The comparison shows that the FEM models are able to approximate close to the same shape but not quite match the results found in the field. This is caused by the FEM deflecting more uniformly.

Additional quantitative analysis results were also produced for the differential deflection for all four cases at midspan using in Figures 5.9 and 5.10. The center LL FEM model matched the differential deflection well with a comparison value of 0.84, but the offset LL did not match well with a value of 0.52. The lower quantitative analysis result for the offset loading is due to the offset FEM model not matching the unanticipated torsional bridge response.

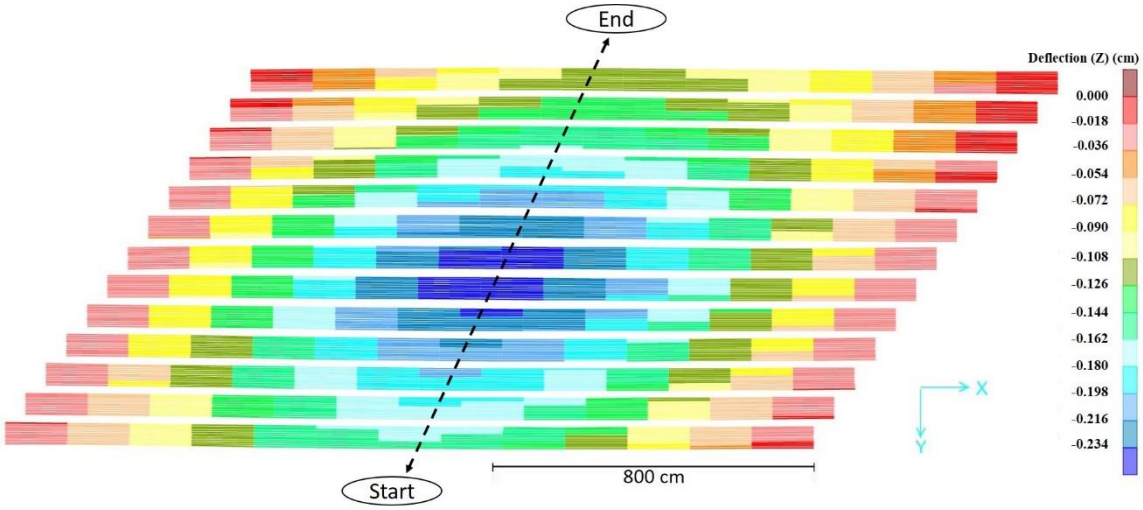

Figure 5.3: CSiBridge model central LL deflection for the girders (cm) (below the bridge viewpoint).

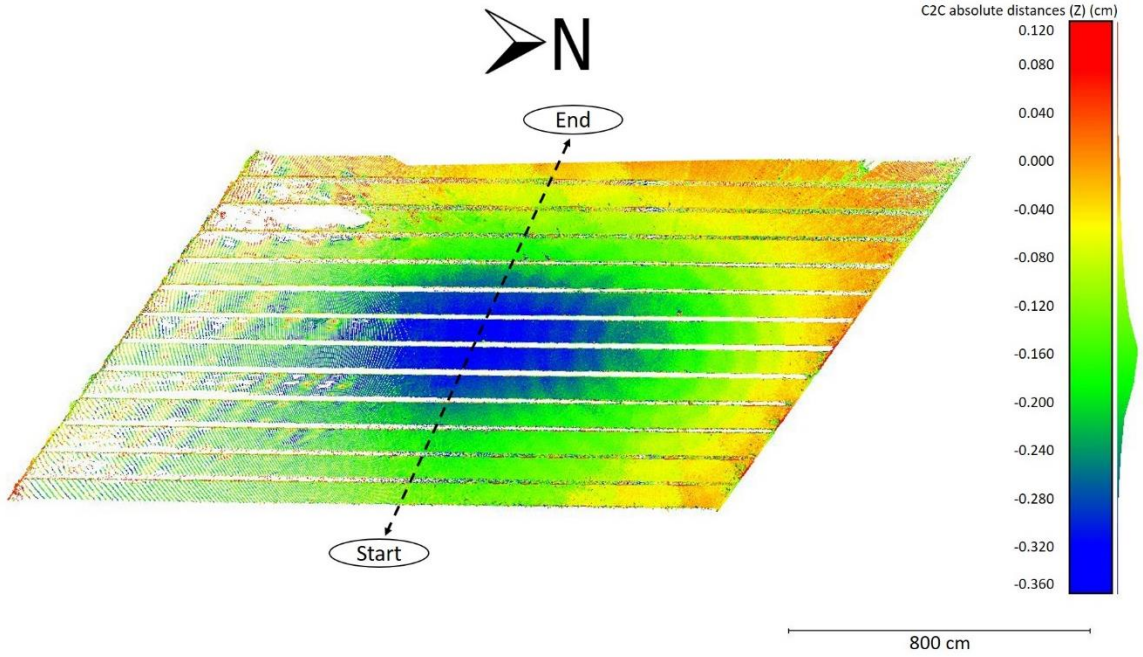

Figure 5.4: C2C distance between DL only and DL plus central LL (cm) (below the bridge viewpoint).

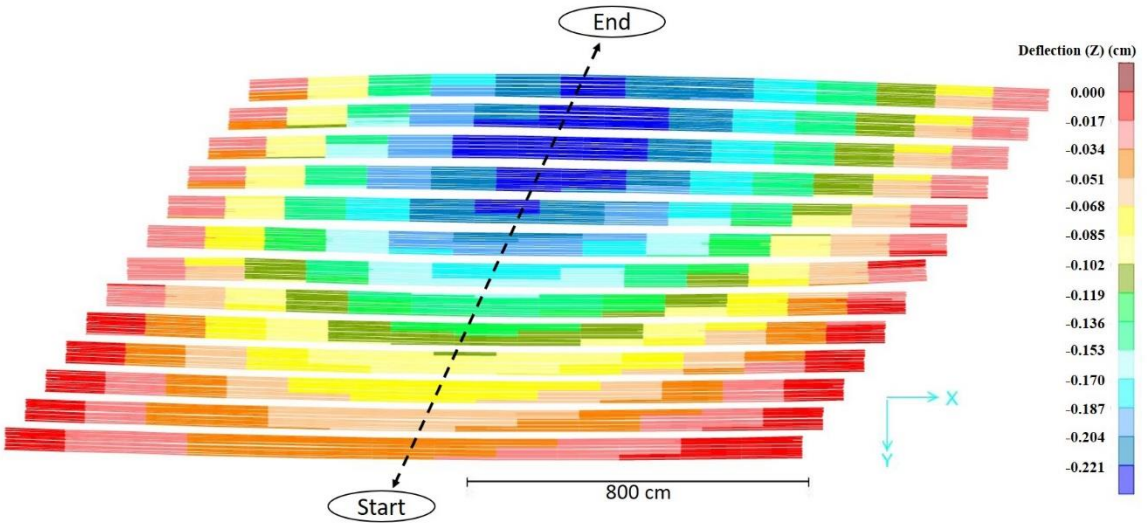

Figure 5.5: CSiBridge model offset LL deflection for the girders (cm) (below the bridge viewpoint).

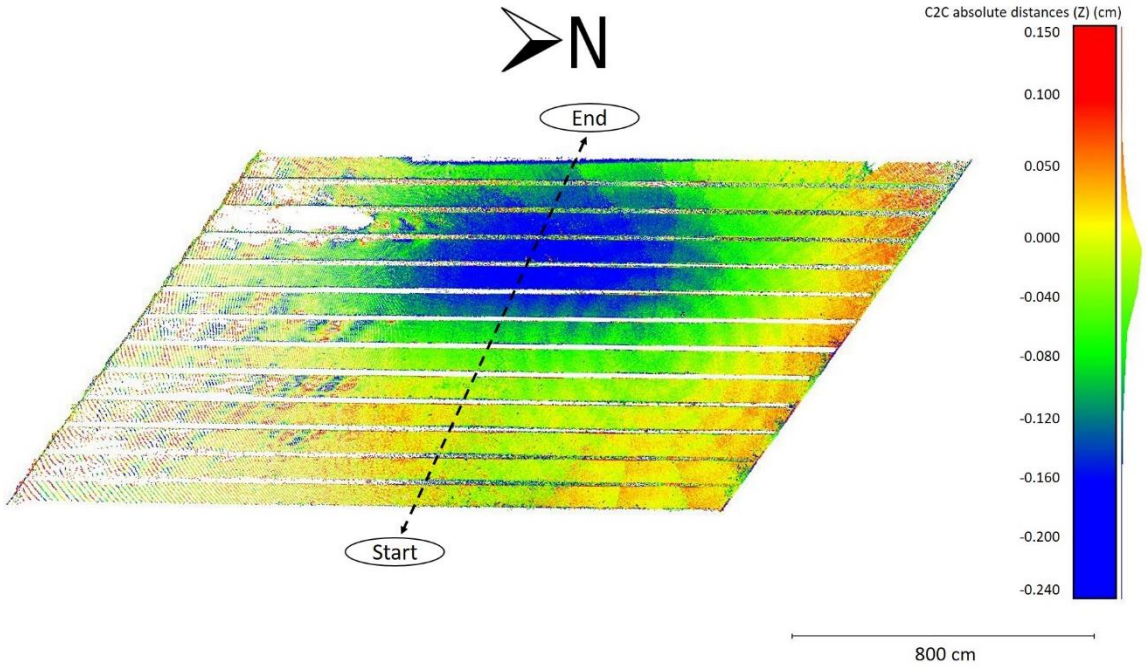

Figure 5.6: C2C distance between DL only and DL plus offset LL (cm) (below the bridge viewpoint).

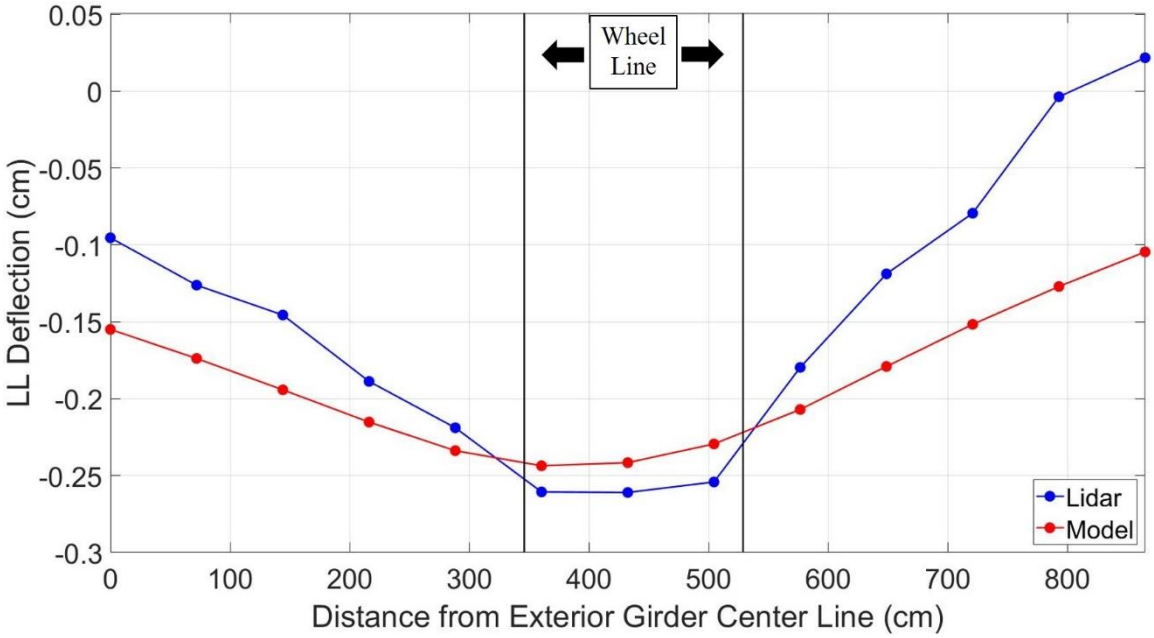

Figure 5.7: Center LL deflection at girder midpoints.

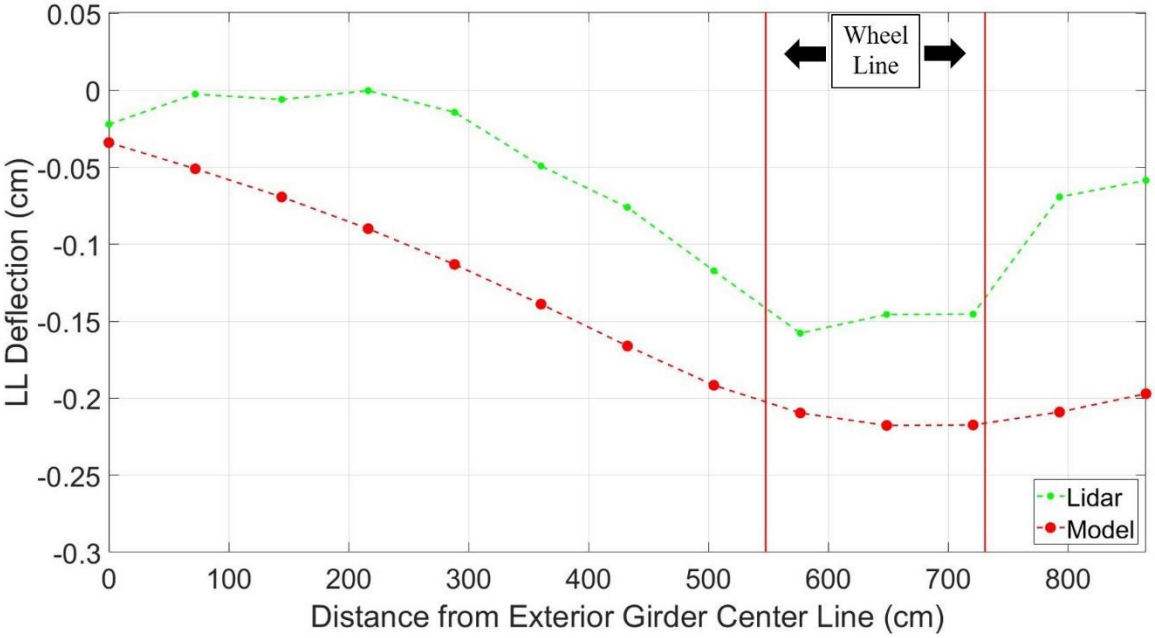

Figure 5.8: Offset LL deflection at girder midpoints.

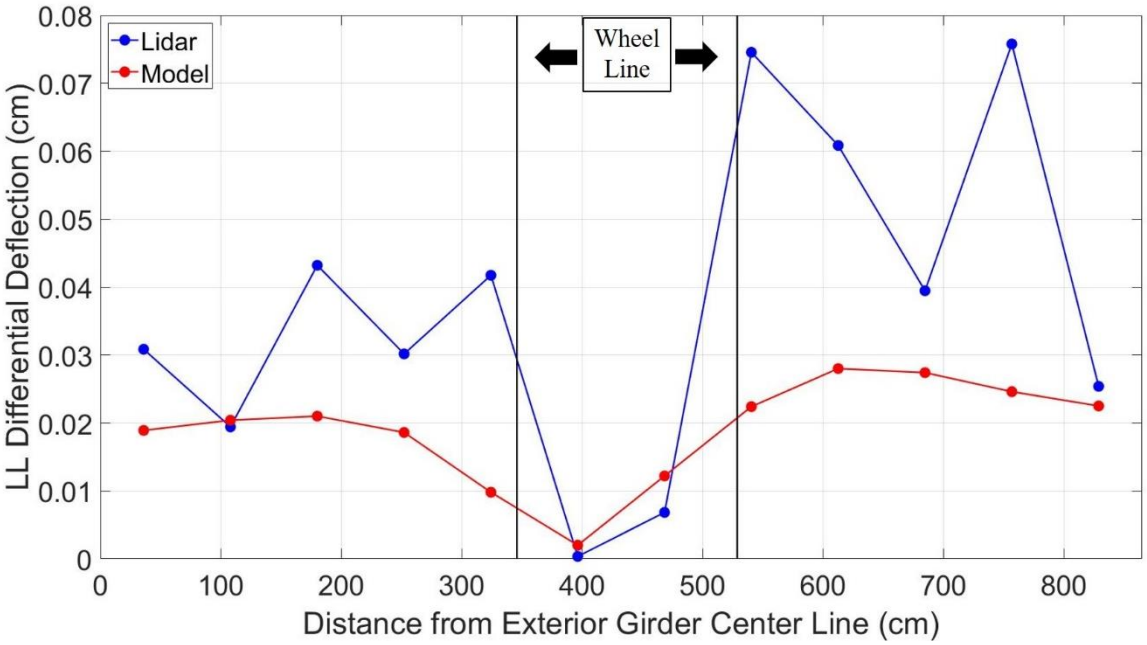

Figure 5.9: Center LL differential deflection between adjacent girders.

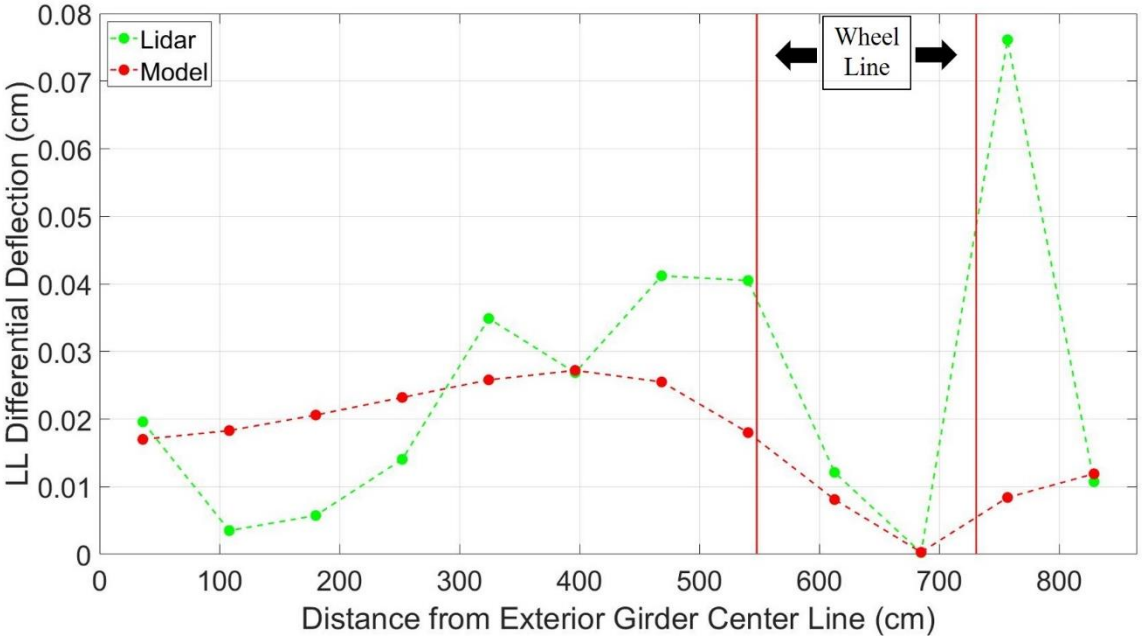

Figure 5.10: Offset LL differential deflection between adjacent girders.

5.4 CONCLUSIONS

The FEM model shows that the model predicts the girders deflecting more uniformly than the response measured in the field. This results in underestimating the maximum deflection for center loading to -0.24 versus -0.26 and overestimating the deflection for offset loading to -0.22 versus -0.16 for the model and lidar, respectively. The model results had a significantly less amount of differential deflection obtaining values of 0.028 and 0.027 cm as compared to 0.076 and 0.076 cm given by lidar for the center and offset loadings, respectively. The level of differential deflection is significant because it can cause problems such as longitudinal deck cracking like in IT girder bridges. Uncalibrated FEM models may have trouble predicting the response for bridges with unique properties such as the IT girder bridge system. Using lidar to calibrate FEM models will likely result in better analysis results.

CHAPTER 6 – CONCLUSIONS

6.1 CONCLUSIONS

The previous chapters summarized conclusions for each of their respective chapters based on the lidar bridge response tests and FEM models. These conclusions identify that lidar assessment can adequately be used for determining bridge response. Additionally, lidar is specifically useful for bridges that will likely have unexpected responses due to asymmetric geometry, unintended torsion for both the global bridge response or the local rotation of individual girders, and/or asymmetric loading. This is because as the bridge or loading becomes more complicated or unpredictable, the model created would become more inaccurate. Narrowly scoped discrete sensors will need a great number of sensors or they will miss part of the bridge response. Ultimately, lidar assessment has proved to be a useful tool for identifying problems with bridge systems and can aid in identifying problems within a system, monitoring deflections during phased construction, or calibrating FEM models.

The live load testing chapter was used to introduce discrete sensors and some of the problems associated with using these methodologies to summarize bridge deflection. While discrete sensors collect data in limited areas and the data can be more difficult to visualize, full-field methods allow for easy interpretation of results and can collect data quicker and easier.

The bridge response chapter tested four bridges and identified that lidar assessment was able to capture bridge responses with a high level of detail. The data collected can be used to calibrate FEM models with difficult to predict parameters. Inaccurate parameters

would likely result in a model with reduced accuracy, which would produce imprecise estimations for distribution factors and load ratings, and not predict problems like excessive deck cracking. Lidar is able to capture girder rotations, which can exacerbate existing problems, as well as provide better insight into how a bridge is responding than what traditional methods are able to do. Additionally, this chapter determined lidar was effective at monitoring bridge response at different stages of phased construction. While phased construction has a lot of uncertainty, it is not often monitored because discrete sensors would have to be rigidly attached throughout the whole process. That type of process could get in the way of construction and result in an overload of data. However, lidar can quickly produce results without getting in the way of construction. The use of these results may provide quick insight into fixing problems associated with phased construction.

The numerical assessment results for a prestressed concrete bridge found that the model predicts the girders to deflect more uniformly than the field measured results. The more uniform response caused underestimation for the max deflection for the center loading and overestimating for the max deflection for the offset loading. Due to the uniformity, the model produced significantly less differential deflection for both the center and offset loadings. Differential deflection is noteworthy because it can cause problems such as longitudinal deck cracking as it did in the IT girder bridge system. This error in modeling shows how uncalibrated FEM models may have trouble predicting the bridge response, especially for bridges with unique features and/or atypical loading. Calibrating FEM models using lidar by adjusting model inaccuracies such as boundary conditions, dimension errors, unintended composite action, and lower bound concrete strength will

likely achieve better analysis results leading to more accurate load ratings and distribution factors for bridges in a more time-efficient way than discrete sensors.

6.2 FUTURE WORK

This thesis has concluded that lidar assessment can be an effective tool for the evaluation and understanding of bridge response. However, its implementation may be improved to get better results. The following research topics are suggested to further study improvements for the use of lidar with change detection:

1. Compare differential deflection and adjacent differential deflection measured with lidar to those measured with an LVDT or precise leveling to determine accuracy. This was out of the scope of this thesis due to site access limitations.
2. Investigate the accuracy of registration by using point-based correspondence versus feature-based correspondence to register the loaded scan to the unloaded scan. An example of using feature-based correspondence is using a plane shape on the bridge abutments to align the scans. The accuracy can be measured by comparing the lidar deflections with the deflections measured by LVDT or precise leveling.
3. Develop calibrated FEM models to account for details like deck cracking, secondary bridge elements such as barriers, and springs for the abutments. Validate the accuracy of calibrated models by testing how accurately they can predict the dynamic response of bridges using equipment such as accelerometers and strain gauges.

REFERENCES

ACI (American Concrete Institute). (2011). Guide to evaluation of strength test results of concrete.

Albert, J., Maas, H., Schade, A., & Schwarz, W. (2002). Pilot studies on photogrammetric bridge deformation measurement. Paper presented at the *Proceedings of the 2nd IAG Commission IV Symposium on Geodesy for Geotechnical and Structural Engineering*, 21-24.

ASCE. (2017). 2017 infrastructure report card.

Azizinamini, A. (2003). Development of a design guideline for phase construction of steel girder bridges.

Besl, P. J., & McKay, N. D. (1992). Method for registration of 3-D shapes. Paper presented at the *Sensor Fusion IV: Control Paradigms and Data Structures, 1611* 586-606.

Chung, W., & Sotelino, E. D. (2006). Three-dimensional finite element modeling of composite girder bridges. *Engineering Structures, 28*(1), 63-71.

CSI. (2016). *Analysis reference manual for SAP2000, ETABS, SAFE and CSiBridge*. Berkeley, California.: Computer & Structures Inc.

Faro. (2011). *Faro laser scanner focus 3D: Features, benefits & technical specifications*. Lake Mary, FL: FARO Technologies.

Fu, Z., & He, J. (2001). *Modal analysis* Elsevier.

Girardeau-Montaut, D. (2015). CloudCompare version 2.6. 1 user manual. *On Line at: Http://Www.Danielgm.Net/Cc/Doc/qCC/CloudCompare% 20v2, 6*, 20.

Girardeau-Montaut, D., Roux, M., Marc, R., & Thibault, G. (2005). Change detection on points cloud data acquired with a ground laser scanner. *International Archives of Photogrammetry, Remote Sensing and Spatial Information Sciences, 36*(part 3), W19.

Hodson, D. J., Barr, P. J., & Pockels, L. (2012). Live-load test comparison and load ratings of a posttensioned box girder bridge. *Journal of Performance of Constructed Facilities, 27*(5), 585-593.

Hughes, T. J. (2012). *The finite element method: Linear static and dynamic finite element analysis* Courier Corporation.

Jaber, F. (2013). Nebraska's inverted tee short-span bridge system. *Pci Aspire*, (Spring 2013), 34-35.

Jaboyedoff, M., Oppikofer, T., Abellán, A., Derron, M., Loye, A., Metzger, R., & Pedrazzini, A. (2012). Use of LIDAR in landslide investigations: A review. *Natural Hazards, 61*(1), 5-28.

James, M. R., & Robson, S. (2012). Straightforward reconstruction of 3D surfaces and topography with a camera: Accuracy and geoscience application. *Journal of Geophysical Research: Earth Surface, 117*(F3)

Kamel, M. R., & Tadros, M. K. (1996). The inverted tee shallow bridge system for rural areas. *PCI Journal, 41*(5)

Lague, D., Brodu, N., & Leroux, J. (2013). Accurate 3D comparison of complex topography with terrestrial laser scanner: Application to the rangitikei canyon (NZ). *ISPRS Journal of Photogrammetry and Remote Sensing, 82*, 10-26.

Liao, Y., Mohammadi, M. E., Watson, D. P., Wood, R. L., Song, C. R., & Kim, Y. (2019). *Applications of LiDAR for SDDOT.* ().South Dakota Department of Transportation.

Liu, W. (2010). Terrestrial LiDAR-based bridge evaluation. *Dissertation Abstracts International, 71*(06).

Lõhmus, H., Ellmann, A., Märdla, S., & Idnurm, S. (2018). Terrestrial laser scanning for the monitoring of bridge load tests–two case studies. *Survey Review, 50*(360), 270-284.

Martindale, G., Watson, D., Kodsy, Antony Mohsen Kamal Masoud, El-Khier, M. A., Wood, R. L., & Morcous, G. (2019). *Performance evaluation of inverted tee (IT) bridge system.*

Martindale, G. P. (2018). Structural identification and assessment of the inverted tee girder bridge system.

Pastor, M., Binda, M., & Harčarik, T. (2012). Modal assurance criterion. *Procedia Engineering, 48,* 543-548.

Raugust, J. D., & Olsen, M. J. (2013), Emerging technology: Structure from motion. *LiDAR Magazine.*

Roddenberry, M. R., Chipperfield, J., & Tawfiq, K. S. (2011). Effect of secondary elements on load distribution in prestressed bridge girders. Paper presented at the *Structures Congress 2011,* 215-226.

Rusu, R. B., Marton, Z. C., Blodow, N., Dolha, M., & Beetz, M. (2008). Towards 3D point cloud based object maps for household environments. *Robotics and Autonomous Systems, 56*(11), 927-941.

Sanayei, M., Phelps, J. E., Sipple, J. D., Bell, E. S., & Brenner, B. R. (2011). Instrumentation, nondestructive testing, and finite-element model updating for bridge evaluation using strain measurements. *Journal of Bridge Engineering, 17*(1), 130-138.

Schlune, H., Plos, M., & Gylltoft, K. (2009). Improved bridge evaluation through finite element model updating using static and dynamic measurements. *Engineering Structures, 31*(7), 1477-1485.

Shahrooz, B. M., Ho, I. K., Aktan, A. E., De Borst, R., Blaauwendraad, J., Van der Veen, C., . . . Miller, R. A. (1994). Nonlinear finite element analysis of deteriorated RC slab bridge. *Journal of Structural Engineering, 120*(2), 422-440.

Soudarissanane, S. S. (2016). The geometry of terrestrial laser scanning; identification of errors, modeling and mitigation of scanning geometry.

Szerszen, M. M., Linzell, D. G., Azam, S. E., Al-Hajami, A., Steelman, J., & Wood, R. L. (2019). *Protocol to evaluate and load rate existing bridges.* Mid-America Transportation Center.

Vosselman, G., & Maas, H. (2010). *Airborne and terrestrial laser scanning* CRC press.

Wood, S. L. (1992). *Evaluation of the long-term properties of concrete* Portland Cement Association Skokie.

Zokaie, T. (2000). AASHTO-LRFD live load distribution specifications. *Journal of Bridge Engineering, 5*(2), 131-138.